arXiv:1505.01496v1 [astro-ph.SR] 6 May 2015

PHOTOMETRIC VARIABILITY IN THE CSTAR FIELD: RESULTS FROM THE 2008 DATA SET

Songhu Wang[1], Hui Zhang[1], Xu Zhou[2], Ji-Lin Zhou[1], Jian-Ning Fu[3], Ming Yang[1], Huigen Liu[1], Jiwei Xie[1], Lifan Wang[4], Lingzhi Wang[2], R. A. Wittenmyer[5], M. C. B. Ashley[5], Long-Long Feng[4], Xuefei Gong[6], J. S. Lawrence[5,7], Qiang Liu[2], D. M. Luong-Van[5], Jun Ma[2], Xiyan Peng[2], J. W. V. Storey[5], Zhenyu Wu[2], Jun Yan[2], Huigen Yang[8], Ji Yang[4], Xiangyan Yuan[6], Tianmeng Zhang[2], Xiaojia Zhang[9], Zhenxi Zhu[4], AND Hu Zou[2]

zhouxu@bao.ac.cn, zhoujl@nju.edu.cn

ABSTRACT

The Chinese Small Telescope ARray (CSTAR) is the first telescope facility built at Dome A, Antarctica. During the 2008 observing season, the installation provided long-baseline and high-cadence photometric observations in the i-band for 18,145 targets within 20 deg^2 CSTAR field around the South Celestial Pole for the purpose of monitoring the astronomical observing quality of Dome A and detecting various types of photometric variability. Using sensitive and robust detection methods, we discover 274 potential variables from this data set, 83 of which are new discoveries. We characterize most of them, providing the periods, amplitudes and classes of variability. The catalog of all these variables is presented along with the discussion of their statistical properties.

Subject headings: binaries: eclipsing — catalogs — methods: data analysis — stars: variables: general — surveys — techniques: photometric

[1]School of Astronomy and Space Science and Key Laboratory of Modern Astronomy and Astrophysics in Ministry of Education, Nanjing University, Nanjing 210093, China; zhoujl@nju.edu.cn

[2]Key Laboratory of Optical Astronomy, National Astronomical Observatories, Chinese Academy of Sciences, Beijing 100012, China; zhouxu@bao.ac.cn

[3]Department of Astronomy, Beijing Normal University, Beijing 100875, China

[4]Purple Mountain Observatory, Chinese Academy of Sciences, Nanjing 210008, China

[5]School of Physics, University of New South Wales, NSW 2052, Australia

[6]Nanjing Institute of Astronomical Optics and Technology, Nanjing 210042, China

[7]Australian Astronomical Observatory, NSW 1710, Australia

[8]Polar Research Institute of China, Pudong, Shanghai 200136, China

[9]Department of Astronomy and Astrophysics, University of California, Santa Cruz, CA 95064, USA

1. INTRODUCTION

The study of variable stars has long been an essential part of astronomical research and is the mainstay for understanding stellar properties as well as stellar formation and evolution. Variable stars play a crucial role in such astrophysical pursuits as the age of Universe, the cosmological distance scale, the composition of the interstellar medium and the behavior of the expanding Universe.

Large telescopes are not suitable for studies of low-amplitude variations at high cadence, due to limitations of observing time (Swift et al. 2014), lack of proper instrumentation, and/or insufficient photometric precision (Tonry et al. 2005). In recent years, there has been a rapid progress in the longitude-distributed (e.g., HATNet: Bakos et al. 2004; HATSouth: Bakos et al.2013) and space-based (e.g., *Kepler*: Borucki et al. 2010; *CoRoT*: Baglin et al.2006) transiting surveys providing an enormous amount of high-precision time-resolved photometric data, resulting in a rapidly increasing number of variability detections that are collected by variable star catalogs such as the Variable Star Index[10] (VSX) or the General Catalog of Variable Stars (GCVS, Samus et al. 2012). In addition to these surveys, the variable sky can be efficiently explored by the Antarctic photometric survey.

The extremely cold, dry, steady, transparent, and dark Antarctic winter skies provide favorable conditions for a diverse and extensive range of astronomical observations, including photometric variability detection (Burton 2010, and references therein); The long polar night in Antarctica greatly facilitates the detection of low-amplitude variables with relatively long period which require continuous photometric monitoring. Furthermore, the low levels of atmospheric turbulence at Antarctica results in a decrease in scintillation noise, leading to superior photometric precision (Kenyon et al. 2006). The pre-eminent conditions for photometric observations at Antarctic Plateau have been utilized and quantified by the previous observing facilities conducted at different Antarctic sites: SPOT (Taylor et al. 1988) at the Amundsen-Scott South Pole Station; the small-IRAIT (Tosti et al. 2006), ASTEP-South (Crouzet et al. 2010), and ASTEP-400 (Daban et al. 2010) at Dome C Concordia Station.

Dome A, located $1,200\,\mathrm{km}$ inland on the Antarctic Plateau, is thought to be the coldest place on Earth. At $4,093\,\mathrm{m}$ Dome A is also the highest ice feature of Antarctica. An analysis carried out by Saunders et al. (2009) who considered the weather, precipitable water vapor, the boundary layer, the free atmosphere, aurorae, airglow, thermal sky emission, and surface temperature led them to conclude that Dome A may be the best site on Earth.

[10]http://www.aavso.org/vsx/

With the aim of taking advantage of and quantifying these favorable astronomical observing conditions at Dome A, the Chinese Small Telescope ARray (CSTAR) was shipped and established there in 2008 January. In the same year, approximately 300,000 i-band photometric images were collected during nearly continuous observations for more than four months, resulting in a high-precision catalog (see Figure 1) of 18,145 stars in a field centered on the South Celestial Pole (Zhou et al. 2010a; Wang et al. 2012, 2014a), which makes these data an excellent source for detection of various types of photometric variability.

A first characterization of the stellar variability in the CSTAR field has been published by Wang et al. (2011, 2013). In this paper we present the more fruitful results of a search for variable stars in this field based on the higher-precision light curves, obtained from independent analysis of the CSTAR data set from the observations in 2008.

The layout of the paper is as follows. The CSTAR telescope system setup, the observational strategy and data reduction processes are briefly described in Section 2. In Section 3, we detail the techniques of variable-star detection and period determination. In Section 4, we present and discuss the results of variable-star search in the CSTAR field. Lastly, the work is summarized in Section 5.

2. INSTRUMENT, OBSERVATIONS AND PREVIOUS DATA PROCESSING

2.1. Instrument

CSTAR, controlled from the PLATO autonomous observatory (Lawrence et al. 2009; Yang et al. 2009), consists of four fixed, co-aligned 14.5 cm (effective aperture of 10 cm) telescopes, each with a different optical filter in SDSS bands: *r, g, i* and *open*. Each telescope is equipped with a 1K × 1K Andor DV 435 frame transfer CCD camera with a pixel size of 13 μm and an angular resolution of 15 arcsec pixel^{-1}, yielding a $4^\circ.5 \times 4^\circ.5$ wide field of view (FOV) around the South Celestial Pole. Details of the CSTAR facility can be found in Yuan et al. (2008) and Zhou et al. (2010b).

2.2. Observations

CSTAR, the first photometric telescope to enter operation at Dome A, was successfully deployed there in 2008 January, and operated for the subsequent four winters until it was retrieved in 2012 to be repurposed. The data set analyzed in this work was collected from

2008 March 4 to August 8. In this observing season, about 1728 hr observations provided some 0.3 million i-band frames for 18,145 stars with exposure times of 20 s or 30 s. A detailed description of the CSTAR observations in 2008 is given in Zhou et al. (2010a).

2.3. Previous Data Reduction

To achieve mmag photometric precision for the bright CSTAR objects, the data set was calibrated and reduced using a custom reduction pipeline as described in detail in Zhou et al. (2010a) and Wang et al. (2012, 2014a). Here only the main factors to be considered when reducing the CSTAR data are briefly reviewed.

After the bias and the flat field were corrected, aperture photometry was performed on all CSTAR frames. Using the 48 bright local calibrators, the CSTAR instrumental magnitudes were then calibrated to the SDSS i. Instead of registering every CSTAR photometric catalog to an external astrometric reference catalog, we generated light curves of 18,145 point sources in the fixed CSTAR field by matching all CSTAR photometric catalogs to a master catalog using a triangle matching algorithm (Valdes et al. 1995). The master catalog, constructed from 10,000 CSTAR frames taken in the best photometric conditions, was astrometrically registered to the USNO-B catalog (Monet et al. 2003) by only solving for the frame center and rotation angle, producing relatively large astrometric residuals (The coordinates of identified variables in this study are provided by cross matching against 2MASS catalog : Skrutskie et al. 2006. The original CSTAR coordinates are retained only as the index of the released light curves: Zhou et al. 2010a, Wang et al. 2012, 2014a). After that, the first version of the CSTAR photometric catalog, detailed in Zhou et al. (2010a), was constructed.

For detection of low-amplitude photometric variability, including planetary transits, the first version of the CSTAR photometric products were further refined by employing corrections for additional systematic errors, as outlined below.

For mmag photometry, uneven atmospheric extinction across the large CSTAR FOV ($4.5^\circ \times 4.5^\circ$), especially under bad observing conditions, cannot be ignored; This was modeled and corrected by comparing each CSTAR photometric frame to a master frame. For details on how this refinement was achieved, see Wang et al. (2012) .

The residual of the flat-field correction shows up as daily systematic variations in stellar flux during the diurnal motion of the stars on the static CSTAR optical system. It was effectively corrected by comparing each target object to a bright and constant reference star in the nearby diurnal path. We refer the reader to Wang et al. (2014a) for more details.

3. VARIABLE STAR DETECTION

In this section, we concentrate on the procedures for the variable star detection, beginning with a review of the final photometric precision of the CSTAR data, continuing with a description of the methods used to sift the variables, and finishing with a discussion of the robust techniques adopted to eliminate the false-positive detections.

3.1. Photometric Precision

The resulting light curves from the ensemble photometry stage of our pipeline typically reach a precision of ~ 0.004 mag at 20 s or 30 s cadence for the brightest non-saturated stars ($i = 7.5$), rising to ~ 0.02 mag at $i = 12$. The distribution of the standard deviation of light curves is shown in Figure 1. Each point represents the rms of a 20 s or 30 s sampled light curve with more than one hundred-day observations.

3.2. Detection of Variables

3.2.1. Detection of Variables in General

In this section, we identify possible photometric variability from the CSTAR data set in two steps. The first involves the relation between the light-curve standard deviations and their median i magnitudes as shown in Figure 1. Naturally, the variable stars are expected to present higher deviations than non-variable stars with the same brightness. For that reason an object is tagged as a variable candidate if its standard deviation is three times higher than the typical value at its magnitude.

As pointed out by Rose & Hintz (2007), this method is not sensitive to low-amplitude variables. Moreover, remaining systematic effects or even several problematic data points in the light curve will result in a higher deviation, which can give rise to false-positive variability detection. To further identify variable stars, we employ the Stetson variability index J defined by Stetson (1996) and modified by Zhang et al. (2003) to our data set. The J statistic is given as

$$J = \frac{\sum_{k=1}^{n} \omega_k \mathrm{sgn}(P_k)\sqrt{|P_k|}}{\sum_{k=1}^{n} \omega_k}, \tag{1}$$

where ω_k is the time-related weighting factor assigned to the k^{th} pair of measurements,

calculated by

$$\omega_k = \exp(-\frac{\Delta t_k}{\overline{\Delta t}}), \tag{2}$$

where Δt_k is the time interval for the $k^{\rm th}$ pair of measurements and $\overline{\Delta t}$ is the median time interval for all pairs of measurements. The expression P_k is the product of the normalized residual for the $k^{\rm th}$ pair of measurements and is given by

$$P_k = \frac{n}{n-1}(\frac{m_{1,k} - \overline{m}}{\sigma_{1,k}})(\frac{m_{2,k} - \overline{m}}{\sigma_{2,k}}), \tag{3}$$

where $m_{1,k}$ and $m_{2,k}$ are the first and second magnitudes of the $k^{\rm th}$ pair of measurements, $\sigma_{1,k}$ and $\sigma_{2,k}$ denote the propagated errors associated with these measurements. $\overline{m}$ is the median magnitude, and n is the number of observational pairs. The Stetson J index is small when the normalized magnitude residuals P_k are uncorrelated, as in the case of non-variable stars, even those with high values of standard deviation. Real variable stars have correlated magnitude measurements across pairs of subsequent observations, which will increase the Stetson J index for such sources. It is therefore particularly reliable when checking for correlated variations in subsequent measurements. Figure 2 presents the distribution of the variability index J for all target objects in the CSTAR data set. The empirical limiting value of $J = 0.4$ is applied to distinguish possible variable candidates from non-variable stars.

3.2.2. Further Detection of Periodic Variables

An example of a clear transit event, obtained by the transit search (Wang et al. 2014b) in the CSTAR data set, is shown in Figure 3. The low $J = 0.088$ and rms $= 0.029$ values of this star indicate that both methods described in section 3.2.1 are not effective approaches for detecting low-amplitude periodic variables. In order to maximize the detection yield and to search for periodicities, we perform a further analysis of our data set especially for periodic variables.

Two methods are applied to search for periodic signals among all the CSTAR objects. The analysis of variance (AoV) method, introduced by Schwarzenberg-Czerny (1996), is applied as the first step. In this method, after the light curve is phased and binned with a series of trial periods, the best period is determined to minimize the ratio of the intra-bin to the overall inter-bin variances. Although it is a time-consuming process, the AoV statistic is applied with $N = 7$ harmonics to all the CSTAR objects to obtain power spectra between 0.01 and 100 days. Light curves which show significant AoV statistics (detection threshold > 6) are folded with their respective frequencies and then inspected visually before accepted

as periodic variables. Figure 4 shows as an example the phased light curve of a randomly selected periodic variable found in this manner.

Since this method is not optimal for detecting transit events, a more sophisticated transit-sifting algorithm (BLS, Kovács et al. 2002) is applied to the CSTAR data set to identify three transit-like events (see Figure 3 for example).

3.3. Data Validation

Since the detection products are inevitably affected by the remaining systematic effects presented in the CSTAR data set, additional tests are performed to distinguish spurious signals from the true stellar variability. The variable candidates which meet any of the following criteria are discarded.

- *Frequencies with Poor Phase Coverage.* Gaps or clumpy data points in the phased light curve would lead to aliasing. A visual inspection is made of each detected variable candidate. Surviving variable candidates are required to have smoothly sampled phased light curves.

- *Periods at Known Aliases.* Both AoV and BLS period-search algorithms suffer from aliasing originating from the remaining systematic errors in the CSTAR data set. It generates false period peaks at frequencies associated with 1 d and at some other commonly occurring frequencies. To minimize the number of false-positive detections, objects with detected periods close to known aliases are excluded.

- *Photometric contamination.* False variablity may result from non-variable objects contaminated by the nearby variables. This kind of spurious variables can be eliminated by comparing their light curves to the light curves of nearby sources that can be resolved by the CSTAR images. Note the large pixel scale ($15\,\mathrm{arcsec\,pixel^{-1}}$) of CSTAR would inadvertently leave unresolved blending in the data set, which reqiure follow-up time-series photometry with instrumentation giving high spatial resolution to confirm their variability.

  In addition, in case of uncertainty, the related images are inspected by eye. A hot pixel or cosmic ray can affect the star or sky value used for photometry. The bright wings of saturated stars or a satellite track can also seriously impact the measurements. After detailed visual inspection, 274 objects which show robust variability are finally selected as the reliable variables in the CSTAR field.

4. RESULT AND DISCUSSION

4.1. Result and Statistical Discussion

About 18,145 objects down to $i = 14.8$ are used to detect variability in 20 square degrees of the CSTAR FOV. The variability-searching process finally yields 274 (~ 1.51 percent of the total objects) variables, including 221 with clear periodicity. All these objects along with their detailed information are presented in Table 1 and Table 2. The stellar identifer is of the form 'CSTAR J$hhmmss.ss + ddmmss.s$', based on their coordinates from the first release of the CSTAR photometric data set (Zhou et al. 2010a).

As a summary of our findings for the CSTAR project, histograms of the amplitude, J index, magnitude as well as determined period for the detected variable stars are shown in Figures 5 to 8.

The amplitude distribution (Figure 5) for the identified variables in the CSTAR data set yields a rapid falloff at larger amplitude. A significant number of small amplitude (amplitude ≤ 0.05) variables is detected. Not surprisingly, the fraction of stars that are significantly variable is less than the fraction of stars with small amplitude variability.

Although the variability-detection fraction increases with the J index (upper panel in Figure 6), a number of identified variables with relatively lower J index (bottom panel in Figure 6) indicates that the Stetson variability J index statistic alone is not an effective variable-selection criterion. That is the reason that the multiple detection techniques are adopted in this paper, which significantly increase the efficiency of detection.

The increasing photometric noise in the faint end would lead to a fall in variability-detection fraction. This selection bias is reflected clearly in the fractional distribution of the identified variables as a function of their i magnitude (Figure 7).

We see that the period histogram (Figure 8) for the detected periodic variables yields a somewhat expected distribution. The distribution peaks at slightly less than 3.5 d, and the shorter periods are 5 times more prevalent. Our data set is not sensitive to longer periods, partly due to (1) limitation of the observational time baseline, and (2) the intrinsic frequency of these short-term variables in the entire population of the variables.

4.2. Comparison with Previous Work

CSTAR data collected during both 2008 and 2010 observing season have been independently analyzed and used to detect the variables by Wang et al. (2011, 2013); It provides a

great opportunity to compare and contrast the scientific results of the two groups in detail.

The identified variables in this study are cross-matched with the previous variable catalog (Wang et al. 2011, 2013) from the same data set. We recover 191 of 224 previously known variables. In Table 1, we summarize our recovery attempts in detail. The periods determined by us are generally in agreement with the periods given by Wang et al. (2011, 2013). The improved periods for seven stars which show a clear disagreement in the period determination are checked carefully by reviewing their periodograms and light curves.

Moreover, 83 of our variables have no best counterpart in theirs. These objects are considered as new variables and are summarized in Table 2. These objects, including 60 periodic variables (see Figure 9, phased light curves) and 23 non-periodic or quasi-periodic variables (see Figure 10, light curves), with quite clear variability match our detection criteria very well, but were not reported by Wang et al. (2011, 2013).

On the other hand, we are not able to confirm the photometric variability for 33 targets reported as variables by Wang et al. (2011, 2013). All of these cases are listed in Table 3, and are carefully inspected. It is likely that four of their variability are originating from systematics with the aliased frequencies. The 29 objects show no significant photometric variability at the limits of our detection sensitivity.

4.3. Variability Classification

The variability of stars is usually caused by intrinsic (pulsating, eruptive, cataclysmic) or extrinsic (eclipsing, rotating) factors, or any combination of them.

To assist in the classification of the identified variables in the CSTAR data set, the luminosity classes and spectral types given in the VizieR (Ochsenbein et al. 2000) are utilized, when available. Additionally, the remaining variables are cross-correlated with existing catalogs using a $30''.0$ match radius to provide their JHK magnitudes (2MASS: Skrutskie et al. 2006) and proper motions (PPMXL: Roeser et al. 2010). This allow us to estimate their luminosity classes and spectral types.

We use the $V-K$ color together with the reduced proper motion (RPM; Luyten 1922) to separate the main-sequence dwarfs from giants (Street et al. 2007; Clarkson et al. 2007; Hartman et al. 2011). Here the RPM_V, is calculated as

$$\mathrm{RPM}_V = V + 5\log_{10}(\mu/1000), \tag{4}$$

where the V magnitudes are transformed from their cross-referenced 2MASS JHK magnitudes (Hartman et al. 2011), μ is the proper motion in units of $\mathrm{mas\,yr^{-1}}$ taken from the

PPMXL catalog (Roeser et al. 2010). $\{\mathrm{RPM}_V, (V-K)\}$ space, as displayed in Figure 11, has been shown to be a powerful diagnostic tool in distinguishing dwarfs from giants (Street et al. 2007; Clarkson et al. 2007; Hartman et al. 2011), as the latter lean towards lower values of RPM_V, and higher $V-K$. For the variables without recorded spectral classification, The color indices, derived from 2MASS JHK magnitudes, are used to estimate their expected spectral types (Bessell & Brett 1988). Given the uncertainties inherent in the above analyses which are made from proper motion and color indices alone, these rough estimates are thus not provided in the final variable catalog.

Based on these detailed stellar information together with the noteworthy features (shape, period, and amplitude) of the variable light curves, all the detected variables in our data set are grouped into the following classes according to the GCVS-based schema (Samus et al. 2012).

Pulsating stars are described by δ Scuti type (DSCT), RR Lyrae type (RL), γ Doradus type (GD), Cepheids (CEP), and δ Cephei-type (DCEP) variables. Eclipsing binaries are subdivided into Algol type (EA), β Lyrae type (EB), and W Ursae Majoris type (EW). Some shallow eclipsing signals are identified as transit-like events (TR); Follow-up studies with these stars are needed to confirm whether or not they might be genuine transiting planets. Rotating variables are categorized within the three major groups: BY Draconis-type variables (BY), α^2 Canum Venaticorum variables (ACV), and ellipsoidal variables (ELL). We also introduce a category spotted stars (SP) for the cases showing variability characteristic features of the stellar spots, but the precise type of which could not be determined. In addition, some variables exhibiting unknown features are classified as Irregular variables (IR). This class also includes the cases for which the variable periods appear longer than the observational baseline.

The type of variability assigned to each variable star is presented in Table 1 and 2. The statistic overview of the classification are provided in Table 4.

Finally, we cross match our detections with the *ROSAT* catalog (Voges et al. 1999, 2000) using a $30''.0$ match radius. A total of 12 periodic variables are successfully correlated to the *ROSAT* X-ray sources, including eight of 44 BY Dra stars, three of 23 ellipsoidal variables, and one of 27 Algol type eclipsing binaries, which all are common X-ray emitters (Norton et al. 2007; Christiansen et al. 2008; Hartman et al. 2011). The results of the correlation are included in Table 1 and 2.

Of the 191 recovered variables, our analysis shows that 71 (37%) agree with the classification in Wang et al. (2011, 2013), 108 (57%) previous ungrouped variables are classified, and 12 variables (6%) disagree with the previous category and are reclassified. We are con-

fident that our classification is more reliable, as it is indicated by not only the noteworthy features of the variable light curves, but also their detailed stellar information.

5. CONCLUSIONS

In 2008 polar night, more than four months of high-duty-cycle photometric observations with the Antarctic CSTAR telescope provided long-baseline, high-cadence light curves of 18,145 stars in a 20 $\deg^2$ field centered at the South Celestial Pole.

From this data set we present a catalog of 274 stars exhibiting clear photometric variability, including 83 new variables and 191 already known variables, along with the statistical properties and classification of them. Of all these variables, 58 are eclipsing binaries, 163 are other type periodic variables, and 53 are non-periodic or quasi-periodic variables. It is expected that our knowledge of variables will continue to improve when the CSTAR 2008 data are combined with the multi-band photometric data of subsequent years.

These detections show the favorable quality of Dome A to carry out continuous and long-duration photometric observations, serving a precursor in advance of future photometric surveys conducted at Dome A such as AST3 (Cui et al. 2008) and KDUST (Zhao et al. 2011).

In addition, all of photometric data products, including CSTAR 2008 catalog and light curves for both already known and newly discovered variables, are available online[11].

We thank the anonymous referee for the insightful suggestions that greatly improved this manuscript. This research is supported by the National Basic Research Program of China (Nos. 2013CB834900, 2014CB845704, 2013CB834902, 2014CB845700, and 2014CB845702); the National Natural Science Foundation of China under grant Nos. 10925313, 11333002, 11433005, 11073032, 11003010, 11373033, 11373035, 11203034, and 11203031; the Strategic Priority Research Program: The Emergence of Cosmological Structures of the Chinese Academy of Sciences (Grant No. XDB09000000); the Main Direction Program of Knowledge Innovation of Chinese Academy of Sciences (No. KJCX2-EW-T06); the 985 project of Nanjing University and Superiority Discipline Construction Project of Jiangsu Province; the joint fund of Astronomy of the National Nature Science Foundation of China and the Chinese Academy of Science, under grant Nos. U1231113 and U1231202; the Natural Science Foundation for the Youth of Jiangsu Province (No. BK20130547); and the Jiangsu Province Innovation for Ph.D candidate (No. KYZZ_0030).

[11]http://explore.china-vo.org/.

REFERENCES

Baglin, A., Auvergne, M., Boisnard, L., et al. 2006, 36th COSPAR Scientific Assembly, 36, 3749

Bakos, G., Noyes, R. W., Kovács, G., et al. 2004, PASP, 116, 266

Bakos, G. Á., Csubry, Z., Penev, K., et al. 2013, PASP, 125, 154

Bessell, M. S., & Brett, J. M. 1988, PASP, 100, 1134

Borucki, W. J., Koch, D., Basri, G., et al. 2010, Science, 327, 977

Burton, M. G. 2010, A&A Rev., 18, 417

Christiansen, J. L., Derekas, A., Kiss, L. L., et al. 2008, MNRAS, 385, 1749

Clarkson, W. I., Enoch, B., Haswell, C. A., et al. 2007, MNRAS, 381, 851

Crouzet, N., Guillot, T., Agabi, A., et al. 2010, A&A, 511, A36

Cui, X., Yuan, X., & Gong, X. 2008, Proc. SPIE, 7012, 70122D

Daban, J.-B., Gouvret, C., Guillot, T., et al. 2010, Proc. SPIE, 7733, 151

Hartman, J. D., Bakos, G. Á., Noyes, R. W., et al. 2011, AJ, 141, 166

Kenyon, S. L., Lawrence, J. S., Ashley, M. C. B., et al. 2006, PASP, 118, 924

Kovács, G., Zucker, S., & Mazeh, T. 2002, A&A, 391, 369

Lawrence, J. S., Ashley, M. C. B., Hengst, S., et al. 2009, Review of Scientific Instruments, 80, 064501

Luyten, W. J. 1922, Lick Observatory Bulletin, 10, 135

Monet, D. G., Levine, S. E., Canzian, B., et al. 2003, AJ, 125, 984

Norton, A. J., Wheatley, P. J., West, R. G., et al. 2007, A&A, 467, 785

Ochsenbein, F., Bauer, P., & Marcout, J. 2000, A&AS, 143, 23

Roeser, S., Demleitner, M., & Schilbach, E. 2010, AJ, 139, 2440

Rose, M. B., & Hintz, E. G. 2007, AJ, 134, 2067

Samus N.N., Durlevich O.V., Kazarovets E V., Kireeva N.N., Pastukhova E.N., Zharova A.V., et al., General Catalogue of Variable Stars (Samus+ 2007-2012), VizieR Online Data Catalog: B/gcvs

Saunders, W., Lawrence, J. S., Storey, J. W. V., et al. 2009, PASP, 121, 976

Schwarzenberg-Czerny, A. 1996, ApJ, 460, L107

Skrutskie, M. F., Cutri, R. M., Stiening, R., et al. 2006, AJ, 131, 1163

Stetson, P. B. 1996, PASP, 108, 851

Street, R. A., Christian, D. J., Clarkson, W. I., et al. 2007, MNRAS, 379, 816

Swift, J. J., Bottom, M., Johnson, J. A., et al. 2014, arXiv:1411.3724

Taylor, M., Chen, K.-Y., McNeill, J. D., et al. 1988, BAAS, 20, 952

Tonry, J. L., Howell, S. B., Everett, M. E., et al. 2005, PASP, 117, 281

Tosti, G., Busso, M., Nucciarelli, G., et al. 2006, Proc. SPIE, 6267, 47

Valdes, F. G., Campusano, L. E., Velasquez, J. D., & Stetson, P. B. 1995, PASP, 107, 1119

Voges, W., Aschenbach, B., Boller, T., et al. 1999, A&A, 349, 389

Voges, W., Aschenbach, B., Boller, T., et al. 2000, IAU Circ., 7432, 3

Wang, L., Macri, L. M., Krisciunas, K., et al. 2011, AJ, 142, 155

Wang, L., Macri, L. M., Wang, L., et al. 2013, AJ, 146, 139

Wang, S., Zhou, X., Zhang, H., et al. 2012, PASP, 124, 1167

Wang, S., Zhou, X., Zhang, H., et al. 2014a, Research in Astronomy and Astrophysics, 14, 345

Wang, S., Zhang, H., Zhou, J.-L., et al. 2014b, ApJS, 211, 26

Yang, H., Allen, G., Ashley, M. C. B., et al. 2009, PASP, 121, 174

Yuan, X., Cui, X., Liu, G., et al. 2008, Proc. SPIE, 7012, 70124G

Zhang, X.-B., Deng, L.-C., Xin, Y., & Zhou, X. 2003, cjaa, 3, 151

Zhao, G.-B., Zhan, H., Wang, L., Fan, Z., & Zhang, X. 2011, PASP, 123, 725

Zhou, X., Fan, Z., Jiang, Z., et al. 2010a, PASP, 122, 347

Zhou, X., Wu, Z.-Y., Jiang, Z.-J., et al. 2010b, RAA , 10, 279

This preprint was prepared with the AAS LaTeX macros v5.0.

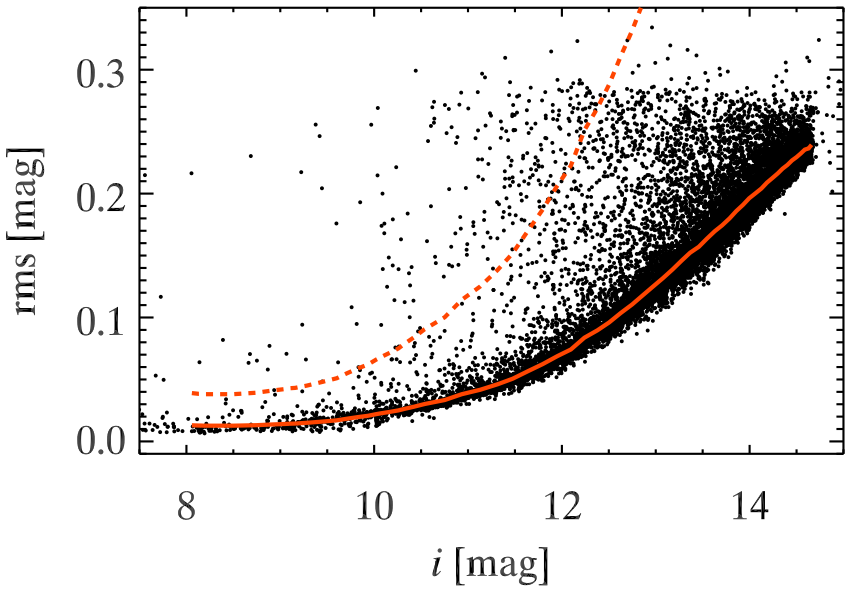

Fig. 1.— Photometric quality of the CSTAR 2008 data set. The standard deviation (20 second or 30 second sampling; 158 day time scale) of each CSTAR light curve is plotted as a fuction of their median i magnitudes. The solid orange line represents the trend of this distribution. Objects above $3\,\sigma$ threshold (the dashed orange line) are tagged as variable candidates.

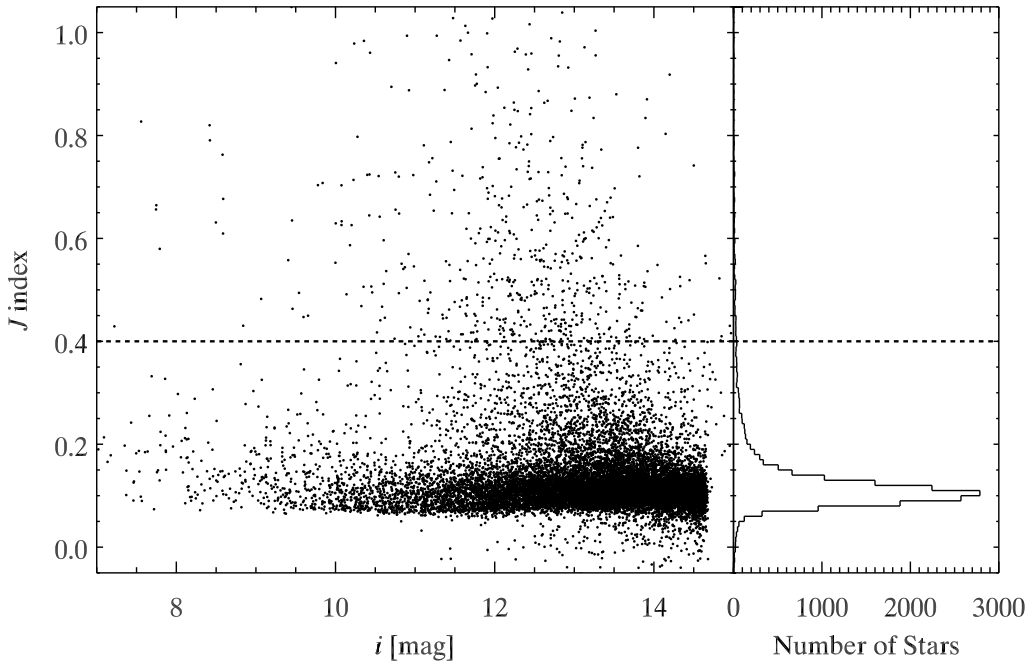

Fig. 2.— Distribution of the Stetson variability J index for all the objects in the CSTAR field. The dashed line marks our threshold for variability detection, $J = 0.4$.

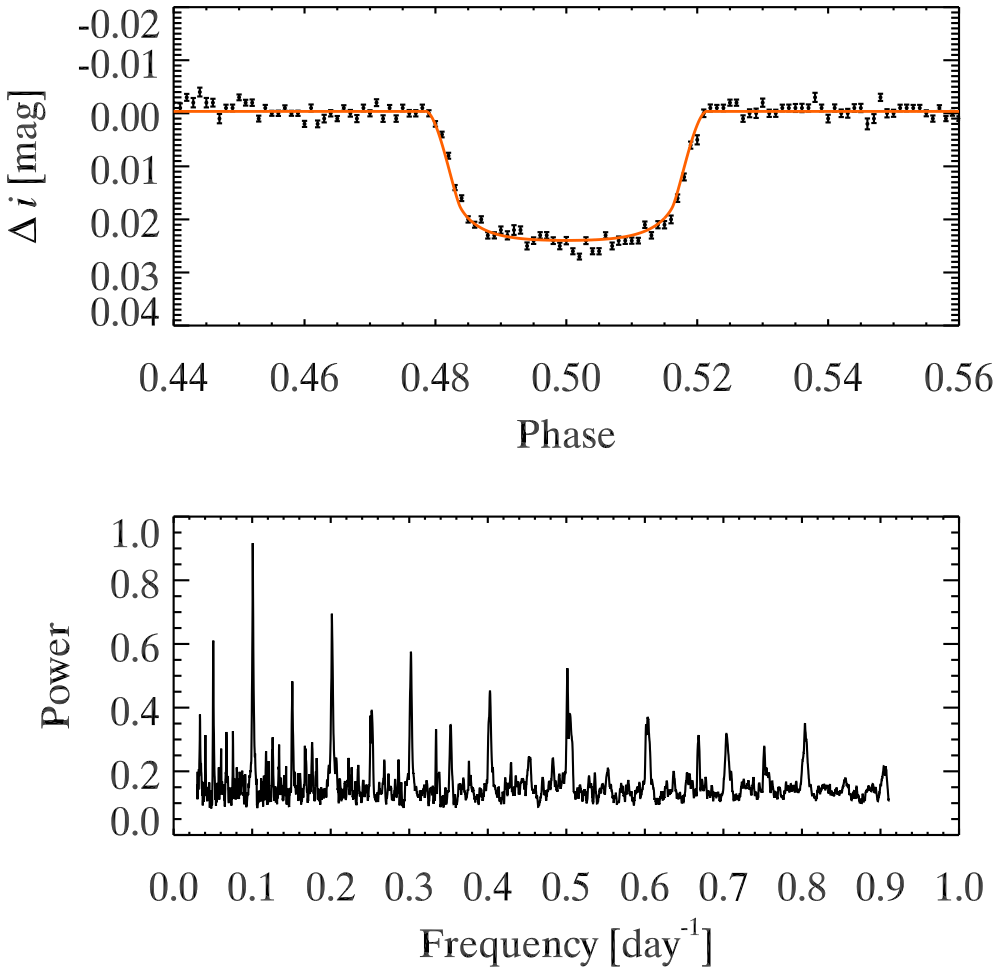

Fig. 3.— Example of a clear low-amplitude variable (CSTAR J183051.60-884322.6) in the CSTAR data set. It cannot be readily identified through the statistical analysis of mag-rms relation or Stetson variability J index due to both low rms = 0.029 and low J index = 0.088 of this star. For that reason, use of AoV and BLS periodic analysis is motivated by the possibility that low-amplitude variables (as in this case) may have potential periodicities which could be reflected in their periodograms (lower panel).

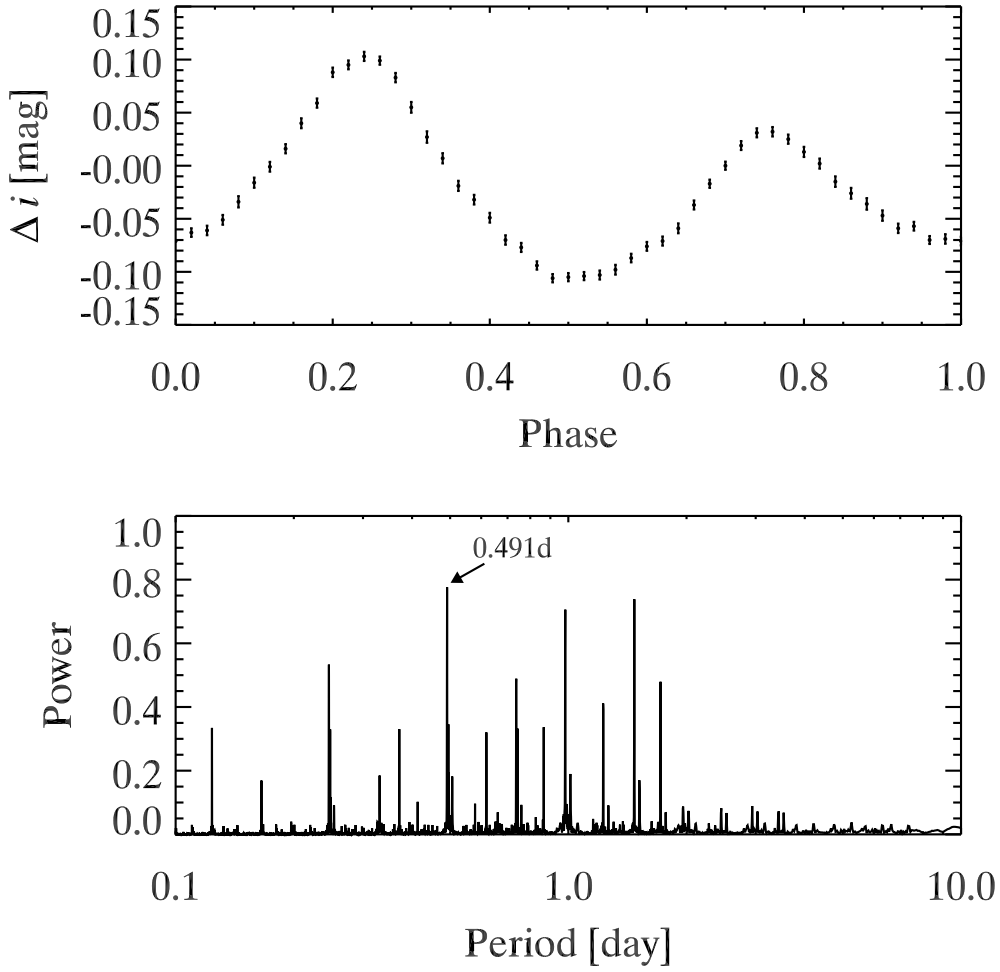

Fig. 4.— Example for one of the periodic variable stars (CSTAR J061948.66-872043.4) detected in this study. The top panel shows the i-band light curve phased on its period of 0.491 days, with AoV periodogram plotted below. The period of this object is indicated by the arrow.

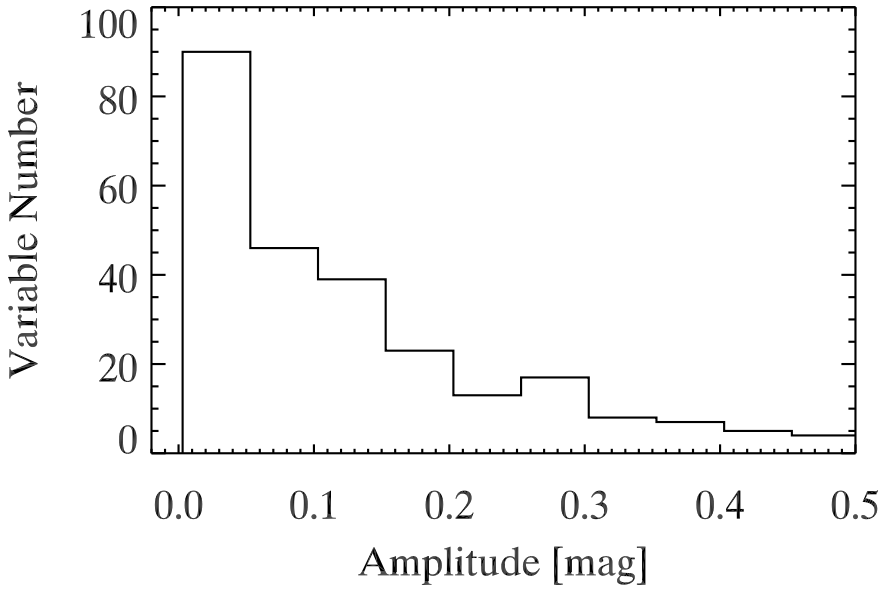

Fig. 5.— Histogram of amplitude for all the variables found in the CSTAR 2008 data set. Note a rough decline from small to large amplitude.

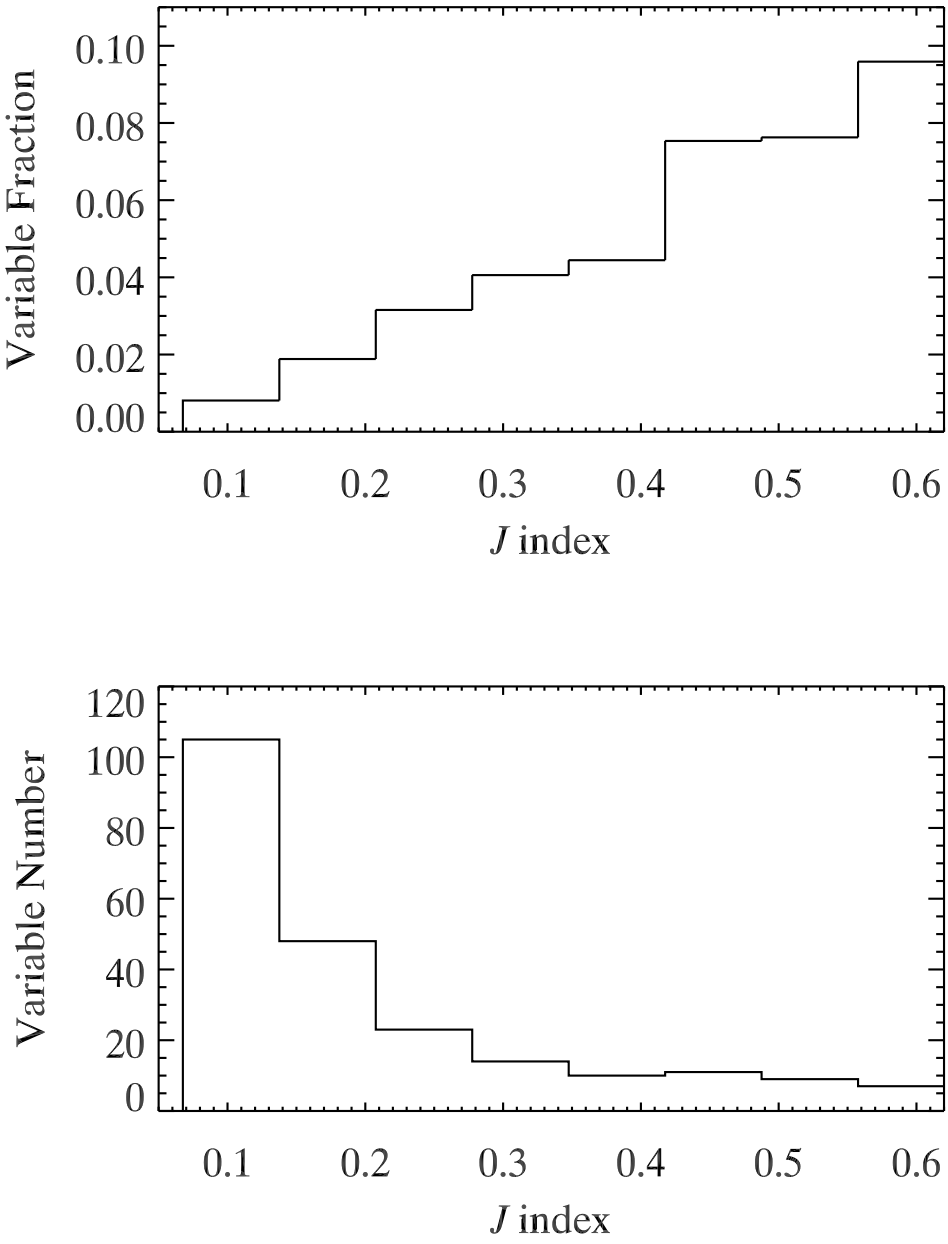

Fig. 6.— (top) Fraction of variable stars as a function of Stetson variability J index. Although the variability-detection fraction increases with the J index, a number of identified variables with relatively lower J index indicates that the Stetson variability J index statistic alone is not an effective variable-selection criterion. The multiple detection techniques are required to ensure the completeness of the detection. (bottom) Distribution in the number of variable stars as a function of J index. Similar to Figure 5, we note an expected decline from small to large J.

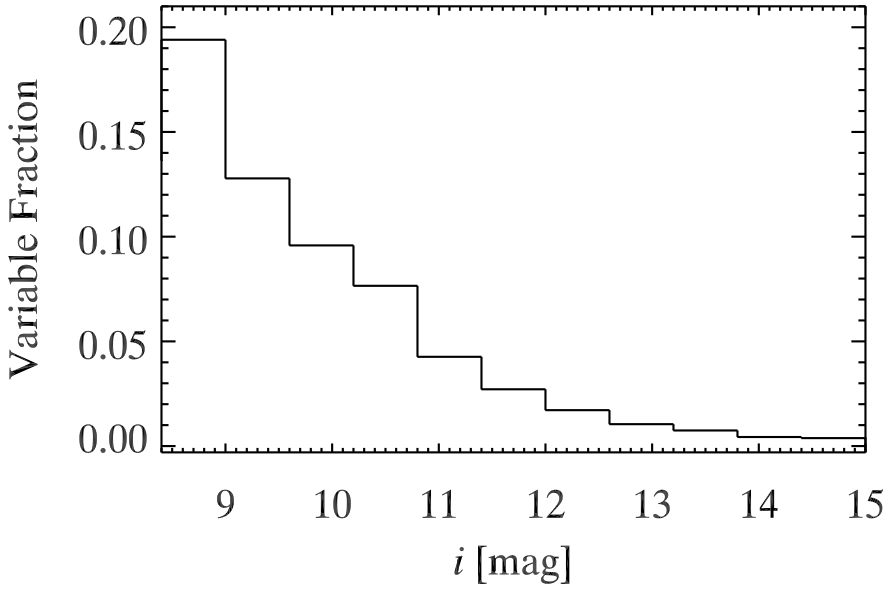

Fig. 7.— Fractional distribution of magnitude for the identified variables in the CSTAR field.

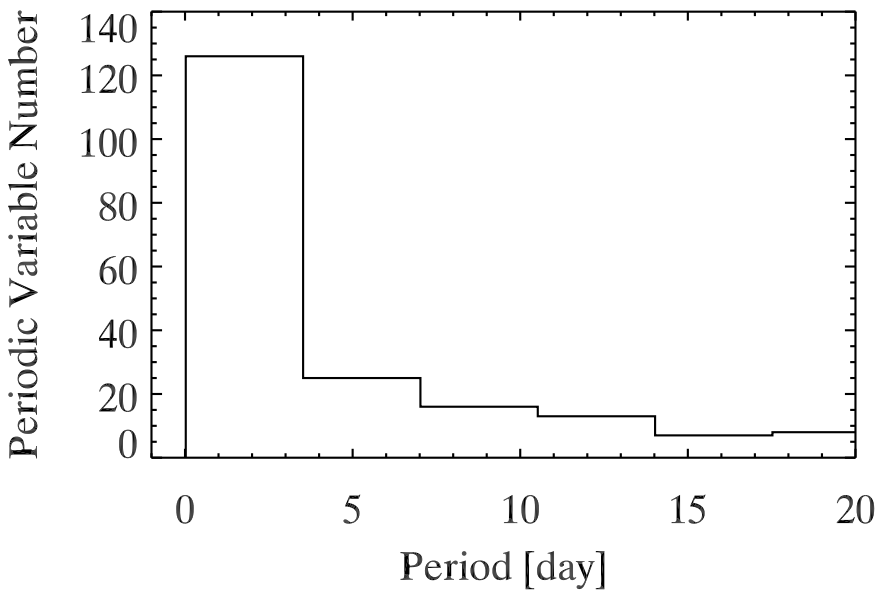

Fig. 8.— Period distribution of the detected periodic variables in the CSTAR 2008 data set. We note a rapid falloff at longer period and a peak in the period of < 3.5 d. Although the efficiency of detecting short-term variables is significantly higher, thanks to more than four-month high-duty-cycle observation during the Antarctic winter, the longest period of detected variables in the CSTAR 2008 data set is up to 88.39 d.

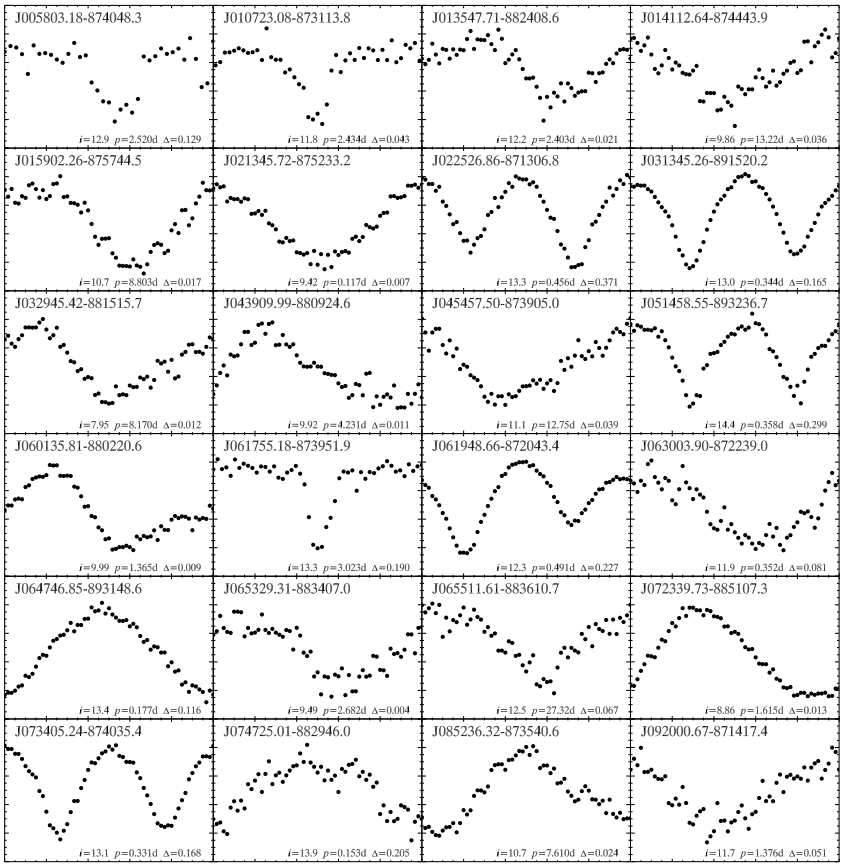

Fig. 9.— i-band phased light curves for 60 periodic variables newly discovered in the CSTAR field, in order of increasing right ascension. The identifer for an object together with its median light-curve magnitude, best-determined period, and maximum peak-to-peak amplitude are shown in each panel.

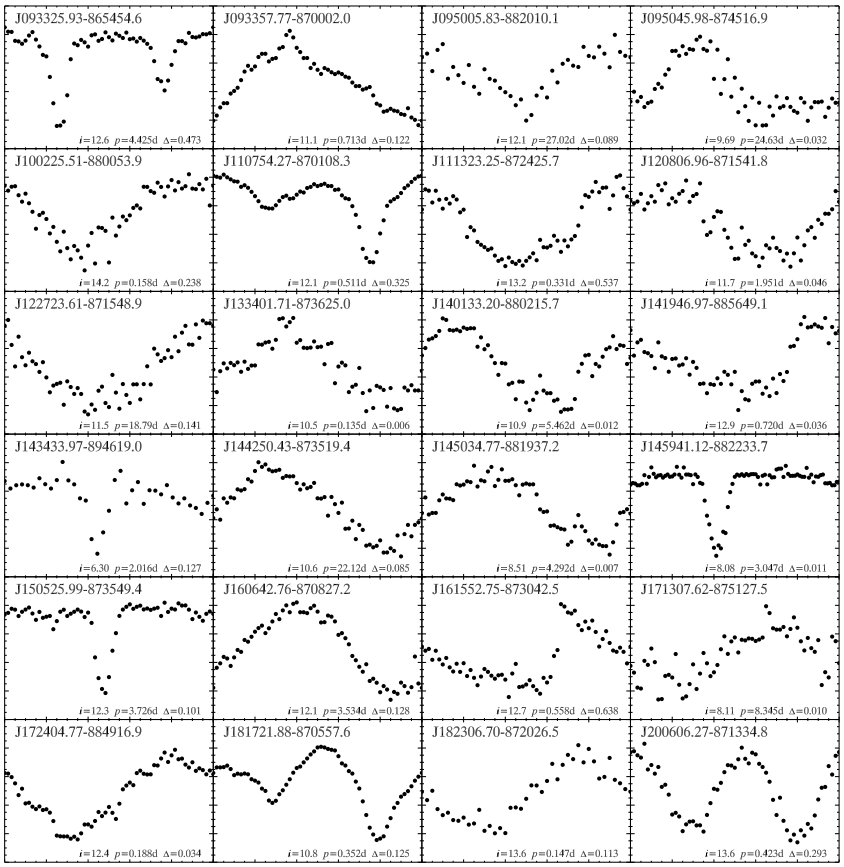

Fig. 9.— Continued

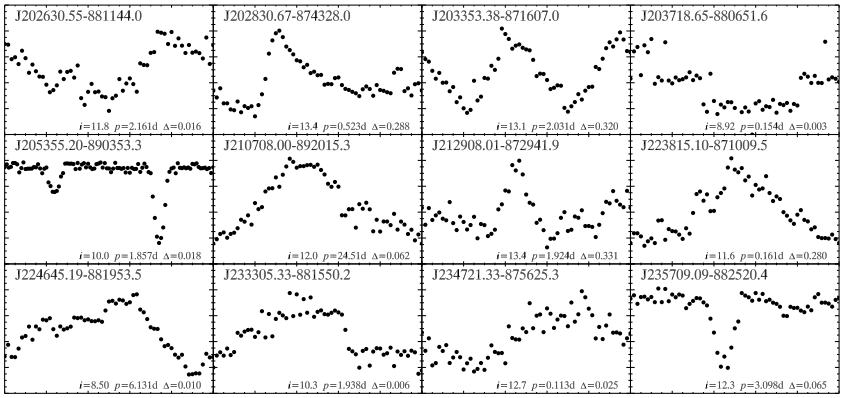

Fig. 9.— Continued

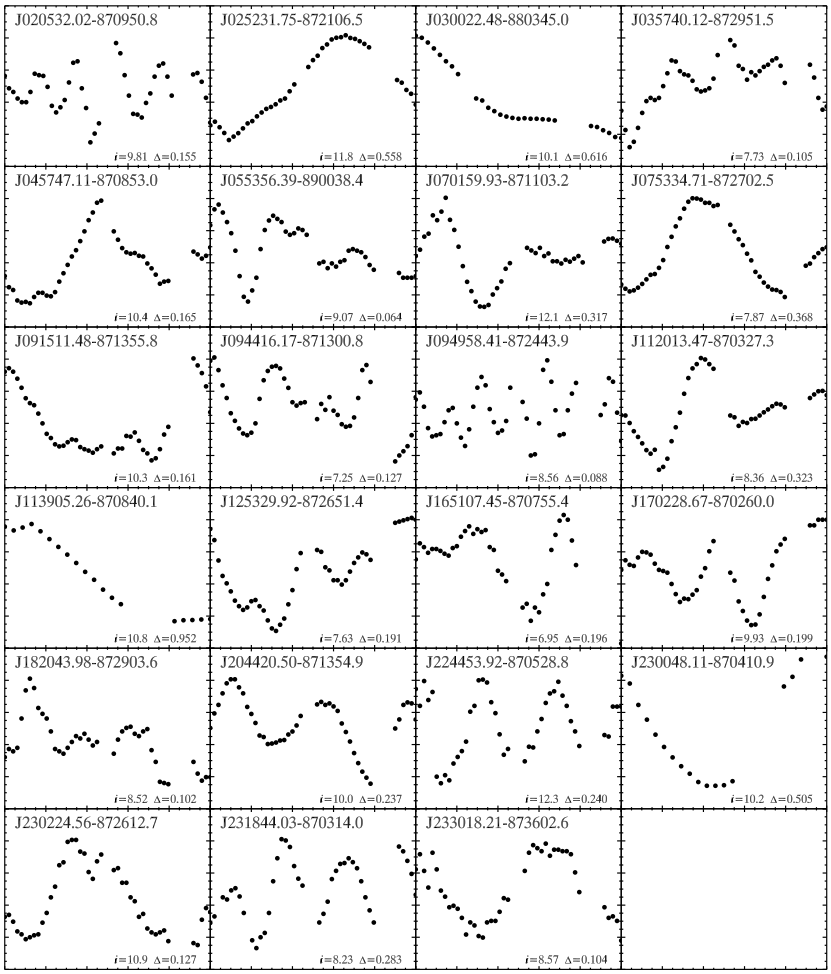

Fig. 10.— i-band light curves for 23 non-periodic or quasi-periodic variables newly discovered in the CSTAR field, in order of increasing right ascension. The identifer for an object together with its median light-curve magnitude and maximum peak-to-peak amplitude are shown in each panel.

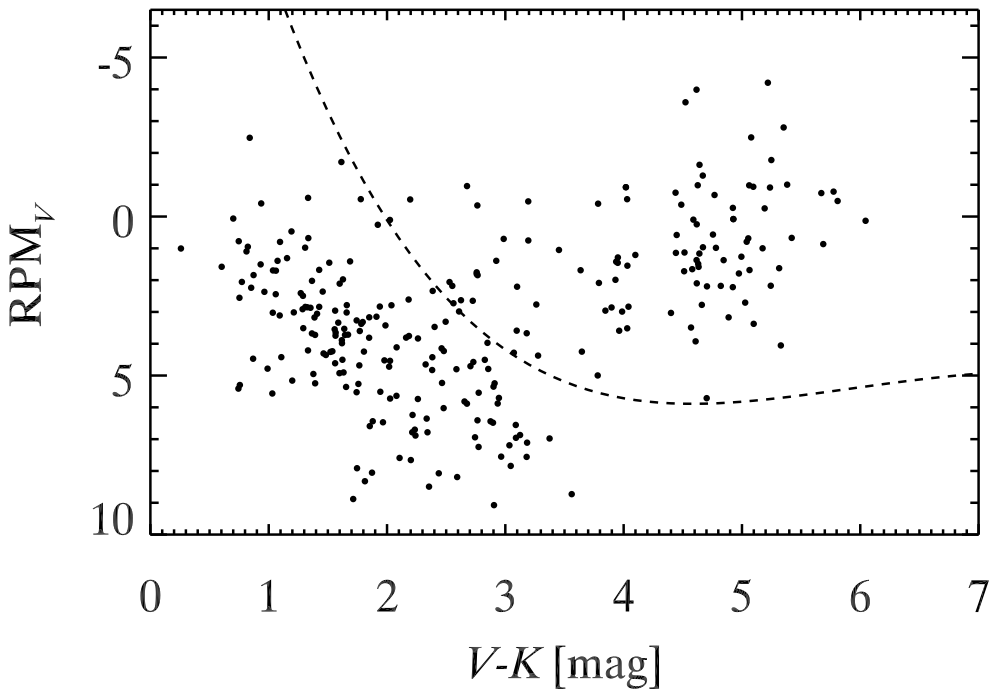

Fig. 11.— $V - K$ vs. reduced proper motion (RPM_V) diagram for the identified variables in the CSTAR field. Giants are separated from dwarfs, as they lean towards lower of RPM_V and higher $V - K$. A polynomial boundary (the dashed line) separating the two groups is taken from Clarkson et al. (2007).

Table 1. Catalog of Recovered Variables from the Previous Study in the CSTAR Field

CSTAR ID CSTAR+	2MASS ID 2MASS+	i (mag)	Period (days)	Amplitude (mag)	T_0 (2454500.0+)	J (mag)	H (mag)	K (mag)	μ_α (mas yr^{-1})	μ_δ (mas yr^{-1})	$T_{\rm eff}$ (K)	Sp.Type	*ROSAT* ID 1RXS+	Type
J000032.66-882011.0	00005088-8819418	9.421	0.1144	0.010	49.2916	8.669	8.572	8.521	13.9	4.9	7134	A4 III	...	DSCT*
J000035.85-875505.0	00005294-8754270	11.622	...	0.733	...	7.061	5.995	5.210	11.0	7.8	...	...	...	IR
J000057.73-874448.1	00011717-8744027	11.892	9.4789	0.440	57.0879	10.983	10.66	10.594	-5.2	-8.1	4664	G8 IV	...	EA
J000826.04-881419.6	00084383-8813479	10.060	...	0.162	...	8.000	7.106	6.814	18.2	0.8	...	...	...	IR
J002022.75-894842.7	00202009-8948378	9.428	10.9234	0.025	56.8881	7.516	6.675	6.389	2.4	4.2	4763	M3 III	...	SP*
J002429.26-890902.3	00243762-8908470	12.600	4.2317	0.050	52.0417	12.097	11.679	11.529	45.9	69.8	...	...	...	BY*
J002951.87-893028.7	00300000-8930198	11.249	0.1527	0.009	49.2987	9.557	8.799	8.581	8.2	9.8	...	...	...	ELL*
J003101.00-885536.1	00311591-8855180	10.780	9.4220	0.010	53.1070	9.887	9.595	9.533	-18.8	-0.2	...	...	...	ELL*
J004559.32-893143.8	00460657-8931348	10.380	5.3650	0.009	50.3104	8.663	7.893	7.652	15.1	10.9	3743	M1 III	...	ELL*
J005237.94-891744.3	00524246-8917319	13.961	0.2930	0.356	49.4712	12.795	12.265	12.173	4.8	-18.2	...	...	...	EW
J005315.20-881315.5	00532724-8812409	13.325	3.5354	0.068	51.7372	11.953	11.322	11.156	44.1	0.3	...	...	...	TR
J005531.82-880946.9	00554594-8809109	11.128	10.7000	0.029	58.1186	9.885	9.308	9.150	-7.0	2.1	4772	K0 III	...	SP*
J012242.85-891715.4	01230217-8917091	13.533	0.1935	0.164	49.3491	13.155	12.839	12.820	-12.0	7.5	...	...	...	DSCT
J015123.86-883352.9	01513454-8833270	11.989	10.8824	0.020	50.5425	11.037	10.72	10.612	11.4	-10.8	5345	G5 V	...	SP*
J020306.98-885549.8	02031012-8855312	12.023	0.4448	0.017	49.4505	11.256	11.095	11.050	5.1	6.2	5953	F6 V	...	GD*
J021252.04-881425.9	02125619-8813524	9.995	12.1160	0.017	57.8934	8.267	7.487	7.241	19.1	7.3	3760	M1 III	...	SP*
J021807.39-875652.7	02181176-8756107	10.504	...	0.148	...	8.390	7.530	7.220	-2.0	8.6	...	...	...	IR*
J022958.24-883459.0	02295840-8834347	14.157	2.8529	0.114	50.6049	13.312	12.799	12.608	38.8	34.0	...	...	...	BY*
J024153.50-882630.9	02415412-8826028	10.954	11.2046	0.012	51.1958	10.058	9.692	9.625	-21.4	-10.8	5764	G5 V	...	SP*
J024226.67-880457.7	02422779-8804223	9.500	...	0.114	...	7.172	6.268	5.979	8.9	7.4	...	...	...	IR*
J024659.89-874751.2	02470229-8747069	11.593	3.6934	0.026	52.5597	10.665	10.356	10.339	15.18	8.36	5200	F8 V	...	ELL*
J025523.56-874901.6	02552390-8748186	12.073	1.9261	0.025	49.6570	11.165	10.835	10.823	2.2	9.0	5492	F5 III	...	GD*
J025611.36-891758.5	02555976-8917478	12.489	0.7206	0.038	49.9540	11.595	11.360	11.287	20.8	0.4	...	...	...	GD*
J030033.53-880259.2	03003494-8802599	10.134	...	0.942	...	6.841	6.033	5.620	7.6	2.7	...	...	...	IR
J030215.47-872337.8	03020853-8722529	13.726	44.7737	0.263	58.9174	12.444	11.841	11.675	4.3	22.4	...	...	...	BY*
J030826.86-890645.2	03081867-8906318	12.213	17.2050	0.066	52.4740	10.196	9.287	9.031	9.5	-0.3	...	...	...	SP*
J031107.83-873615.5	03105957-8735376	10.559	...	0.241	...	8.685	7.843	7.569	8.2	14.1	...	...	...	IR
J031403.36-883315.7	03140117-8832524	14.471	1.2088	0.468	49.7277	13.027	12.448	12.275	18.4	26.1	...	...	...	EA
J032251.59-872414.9	03224315-8723341	13.192	0.2633	0.089	49.4082	12.561	12.306	12.219	10.8	8.1	...	...	...	EW*
J033131.20-880452.2	03313012-8804237	14.003	1.4447	0.188	50.6049	13.045	12.526	12.403	30.0	31.6	...	...	...	EA*
J033725.87-883911.4	03371825-8838513	9.442	7.9579	0.010	52.8179	7.511	6.676	6.385	4.4	10.7	5370	M3 III	...	SP*
J035447.55-880319.6	03544057-8802503	11.574	74.0900	0.169	82.2611	10.224	9.604	9.425	7.5	14.5	...	...	...	SP*
J040107.17-881022.7	04005482-8809592	14.289	0.1590	0.086	49.3399	13.405	13.078	13.029	1.9	-6.5	...	...	...	DSCT*
J040252.25-872309.3	04024455-8722262	10.557	...	0.320	...	7.478	6.546	6.161	3.4	-0.6	...	...	...	IR
J042020.74-882527.6	04201275-8825032	12.630	0.3955	0.129	49.6470	11.890	11.685	11.687	19.4	14.4	...	...	...	EW*

Table 1—Continued

CSTAR ID CSTAR+	2MASS ID 2MASS+	i (mag)	Period (days)	Amplitude (mag)	T_0 (2454500.0+)	J (mag)	H (mag)	K (mag)	μ_α (mas yr^{-1})	μ_δ (mas yr^{-1})	$T_{\rm eff}$ (K)	Sp.Type	*ROSAT* ID 1RXS+	Type
J043645.79-872831.5	04363103-8728034	10.929	0.3085	0.021	49.4221	9.667	9.176	9.075	26.6	115.4	4658	K2 V	J043636.0-872755	BY*
J051226.09-874459.3	05121491-8744422	8.450	...	0.150	...	5.836	4.980	4.519	-20.1	-10.8	...	...	...	IR
J051338.18-872005.7	05132951-8719426	12.000	0.3841	0.358	49.4098	11.170	10.889	10.756	-1.5	1.9	...	...	...	EW
J051559.26-880440.3	05154831-8804230	13.095	5.3650	0.149	50.0422	11.765	11.171	11.046	-1.1	10.3	...	...	...	BY*
J054328.37-880417.1	05431919-8804040	10.534	...	0.156	...	8.387	7.514	7.217	-4.2	6.9	...	...	...	IR
J054421.37-883255.7	05434745-8832568	12.507	0.6462	0.073	49.6077	11.514	10.978	10.846	-8.3	-28.5	...	...	...	BY*
J054716.38-875114.6	05470791-8751001	10.206	0.6070	0.017	49.6006	9.490	9.320	9.247	3.5	-16.0	6928	F0	...	GD
J054902.25-883025.0	05485381-8830163	13.953	13.3800	0.190	59.4602	12.952	12.450	12.256	1.6	18.2	...	...	...	BY*
J060255.98-882936.0	06024183-8829249	13.385	1.2720	0.046	49.3547	12.106	11.458	11.226	-27.4	55. 7	...	...	...	BY*
J061036.94-875342.0	06102762-8753326	14.153	2.3074	0.120	49.7179	12.679	12.159	12.037	3.7	-10.2	...	...	...	BY*
J061217.55-872721.2	06120919-8727161	13.862	0.1316	0.127	49.4088	12.568	12.096	12.006	-2.5	7.8	...	...	...	BY*
J062848.56-880247.5	06284195-8802416	12.310	7.2493	0.432	55.2355	11.293	10.924	10.828	9.4	7.6	...	...	...	EA
J063137.10-881137.7	06313103-8811365	12.757	0.2407	0.038	49.4680	10.042	9.459	9.069	-50.5	240.4	...	M5 V	J063058.5-881135	BY*
J064053.56-881525.3	06404718-8815211	11.580	0.4386	0.415	49.4555	10.717	10.451	10.427	5.8	-1.0	4554	G2 V	...	EW
J065012.81-892158.7	06495126-8921583	9.412	...	0.054	...	7.476	6.628	6.345	-1.1	9.0	...	...	...	IR
J070141.69-881704.5	07013743-8817027	9.559	23.4662	0.035	63.0188	7.711	6.824	6.562	2.6	4.5	...	...	...	SP*
J070750.65-880220.8	07075190-8802110	12.785	0.7899	0.051	49.3148	12.105	11.941	11.879	-3.5	4.5	...	...	...	GD*
J071214.01-875119.4	07121379-8751196	12.755	2.6357	0.104	51.8477	11.411	10.808	10.678	0.2	-22.6	...	...	...	BY*
J071659.93-872843.5	07165261-8728561	13.440	0.3831	0.346	50.4954	12.754	12.326	12.210	3.9	28.0	...	...	...	EW
J073915.21-884040.9	07391465-8840408	13.484	1.4419	0.088	50.6969	11.015	10.452	10.159	-114.4	254.0	...	...	J073856.5-884049	BY*
J074359.59-890736.8	07435276-8907369	12.456	0.7980	0.427	49.3230	11.773	11.500	11.418	0.8	5.0	...	...	...	EW
J074635.95-893960.0	07461396-8940011	10.268	21.6400*	0.034	53.5109	8.218	7.359	7.053	-26.5	10.1	...	...	...	SP*
J075444.90-891540.2	07543806-8915409	9.761	...	0.049	...	7.723	6.827	6.511	1.2	8.6	...	...	...	IR
J080222.20-881420.0	08022559-8814257	13.297	0.2856	0.074	49.4853	12.638	12.387	12.391	6.2	26.1	...	...	...	EW*
J080503.67-890753.3	08050281-8907546	12.917	1.0713	0.085	49.4250	11.968	11.569	11.473	1.1	-16.1	...	...	...	SP*
J080842.25-875955.3	08084572-8800016	13.635	0.8228	0.117	49.5749	12.566	11.950	11.774	19.5	18.6	...	...	...	EA
J081711.62-883725.5	08171558-8837292	14.000	9.3864	0.173	52.2478	12.739	12.236	12.127	-6.6	11.7	...	...	...	BY*
J083920.40-880318.8	08393942-8803193	12.790	1.0484	0.103	50.0040	11.617	11.07	10.872	-15.8	42.6	...	...	...	BY*
J083933.06-873843.5	08394100-8739016	12.152	7.1600	0.223	50.0429	11.078	10.636	10.530	12.4	63.1	...	...	...	EA
J084016.96-884655.4	08402733-8847003	13.751	13.0123	0.318	52.5441	13.324	12.602	12.466	-9.0	-14.3	...	...	...	EB
J084020.90-872819.2	08403344-8728384	12.620	61.3050	0.399	82.7023	10.463	9.527	9.264	3.9	22.0	...	...	...	DCEP*
J084600.83-883334.3	08461143-8833427	11.851	0.2671	0.517	49.3164	10.683	10.107	9.948	-29.8	26.3	...	...	...	EW
J085332.01-882624.2	08534459-8826328	12.376	0.2582	0.052	49.4124	11.151	10.561	10.430	-17.1	10.4	...	...	...	BY*
J090210.28-873720.5	09022063-8737409	12.352	1.6274	0.086	49.6654	11.713	11.605	11.561	-4.2	-2.6	7578	F0 V	...	EA*
J090346.80-883301.7	09035917-8833075	11.327	0.8738	0.222	49.4833	10.540	10.309	10.230	1.5	-3.4	5732	F8 V	...	EA*

Table 1—Continued

CSTAR ID CSTAR+	2MASS ID 2MASS+	i (mag)	Period (days)	Amplitude (mag)	T_0 (2454500.0+)	J (mag)	H (mag)	K (mag)	μ_α (mas yr^{-1})	μ_δ (mas yr^{-1})	$T_{\rm eff}$ (K)	Sp.Type	*ROSAT* ID 1RXS+	Type
J091003.41-872335.2	09101783-8724061	11.383	74.8111	0.115	81.8339	9.302	8.340	8.047	-3.6	6.1	...	...	...	IR
J092243.03-892934.1	09230033-8929386	13.370	0.1247	0.067	49.3746	12.362	11.766	11.598	-7.4	3.9	...	...	...	BY*
J092912.42-872106.6	09292810-8721397	8.933	...	0.238	...	6.478	5.544	5.194	3.0	-4.8	...	...	...	IR
J092917.77-882954.7	09293914-8830063	11.634	0.6221	0.145	49.8230	10.753	10.185	10.060	64.8	17.9	...	...	...	RL
J094410.09-892814.6	09441361-8928174	10.484	16.0479	0.021	61.7282	9.446	8.910	8.762	-16.9	2.5	4589	K2 III	...	SP*
J094940.97-884121.1	09495658-8841271	14.026	1.7354	0.106	49.8211	12.694	12.133	12.002	-9.8	10.3	...	...	...	BY*
J095118.56-872801.5	09513226-8728326	13.079	0.2409	0.065	49.3922	12.036	11.484	11.359	-13.1	3.0	...	...	...	BY*
J095818.45-882351.0	09583480-8823599	12.780	2.0661	0.120	50.7786	11.887	11.537	11.481	-9.4	1.0	...	...	...	EA
J100101.70-884430.9	10011874-8844367	10.040	43.2050	0.160	87.0954	8.452	7.897	7.663	5.3	-1.1	4557	K2 III	...	EA*
J100102.32-881318.4	10012156-8813309	11.841	0.6522	0.225	49.3139	10.985	10.807	10.786	-3.2	10.4	2085	F6 V	...	EW
J100250.68-875047.4	10031005-8751058	10.592	...	0.535	...	7.564	6.685	6.271	-1.7	4.2	...	...	...	IR*
J100421.76-884019.3	10044016-8840252	9.042	0.0925	0.011	49.3165	8.338	8.191	8.150	-20.8	13.6	6755	F0 V/IV	...	DSCT*
J101236.08-873754.1	10125517-8738229	14.143	0.5915	0.605	49.4615	13.379	13.104	13.003	0.4	11.3	...	...	...	RL
J101432.88-873558.4	10145048-8736239	11.071	8.7870	0.032	53.4209	10.062	9.662	9.607	-33.1	16.3	4969	G5 V	...	ELL*
J102533.51-875320.8	10255432-8753409	9.782	20.9782	0.050	49.5008	7.823	6.865	6.628	-2.7	5.7	5733	M4 III	...	SP*
J103212.73-882453.5	10323140-8825030	13.629	3.5354	0.122	50.2279	12.606	12.288	12.239	3.0	12.2	...	...	...	EA
J103954.44-872857.2	10401567-8729298	11.085	0.8688	0.071	49.9036	9.932	9.369	9.241	-32.7	5.5	...	...	...	EA
J104326.86-872436.5	10434640-8725099	9.657	3.6027	0.059	49.4532	8.828	8.444	8.293	-6.1	1.3	6201	A0 V	...	ACV*
J104836.81-880200.2	10490031-8802173	12.198	19.2180	0.071	49.3871	10.748	10.170	10.048	52.0	-6.3	...	...	...	BY*
J105607.29-875501.8	10562808-8755212	11.931	27.2827	0.054	69.4806	10.492	9.860	9.708	12.3	-7.4	...	...	...	SP*
J110341.97-883756.0	11040452-8838025	13.561	4.8158	0.178	52.5658	12.229	11.692	11.600	-0.9	-6.9	...	...	...	BY*
J111058.96-871721.3	11112067-8718010	13.851	0.1544	0.178	49.3294	12.990	12.659	12.480	39.3	-2.4	...	...	...	DSCT*
J111700.40-883536.4	11170055-8835364	9.191	...	0.130	...	6.906	5.995	5.626	-2.3	0.0	5968	M5 III	...	IR
J111848.34-885338.2	11191173-8853410	12.711	1.8780	0.067	49.9484	11.352	10.718	10.564	-38.7	19.4	...	...	J111742.7-885347	BY*
J114744.32-884949.2	11480896-8849525	10.382	25.7950	0.050	62.5755	8.841	8.108	7.951	-8.4	1.3	4535	K3 III	...	CEP*
J115226.94-882320.2	11525071-8823289	9.184	17.0863	0.019	56.8090	7.415	6.613	6.383	-4.6	4.5	3714	M1 III	...	SP*
J120055.08-883039.8	12011933-8830461	11.154	1.7368	0.013	49.4039	10.351	10.105	10.046	-20.7	0.8	6186	F8 V	...	GD*
J120429.21-872234.1	12044864-8723062	8.797	...	0.269	...	5.740	4.870	4.397	-11.7	-9.1	...	...	...	IR
J120750.83-873513.5	12081137-8735396	11.518	26.5670	0.082	49.6896	10.034	9.336	9.119	-6.1	0.5	...	...	...	SP*
J121232.71-883406.3	12125631-8834115	10.762	9.5900*	0.017	53.6066	9.627	9.127	9.024	21.0	-34.2	4931	K1 IV	...	SP*
J122113.32-875959.8	12213645-8800144	12.124	1.8923	0.296	50.9090	11.499	11.362	11.279	-13.5	3.2	7117	F0 III	...	EA*
J123220.14-872552.7	12324299-8726227	10.926	0.3385	0.526	49.4049	9.901	9.463	9.411	6.1	0.0	4308	G5 III	...	EW
J123402.50-873411.8	12342517-8734377	10.121	17.2516	0.038	61.5395	8.098	7.240	6.953	-11.2	-1.1	...	...	...	SP*
J123555.47-890402.9	12362296-8904032	10.973	13.6900*	0.034	52.6451	9.213	8.415	8.187	-16.9	-6.7	...	...	...	SP*
J123935.36-874114.3	12395808-8741374	11.645	...	0.139	...	9.637	8.726	8.442	-6.2	-1.8	...	...	...	IR

Table 1—Continued

CSTAR ID CSTAR+	2MASS ID 2MASS+	i (mag)	Period (days)	Amplitude (mag)	T_0 (2454500.0+)	J (mag)	H (mag)	K (mag)	μ_α (mas yr^{-1})	μ_δ (mas yr^{-1})	$T_{\rm eff}$ (K)	Sp.Type	*ROSAT* ID 1RXS+	Type
J124121.71-875813.3	12414403-8758284	11.394	2.9457	0.055	52.1631	10.09	9.599	9.444	-15.3	1.4	4729	K0 III	...	ELL*
J124308.72-875314.1	12433114-8753309	11.220	23.8193	0.159	52.0303	9.932	9.366	9.203	22.7	35.7	3914	K4 V	...	BY*
J124856.67-881107.8	12491818-8811174	13.784	0.1762	0.278	49.3448	12.747	12.388	12.309	-55.1	41.9	...	...	...	EW*
J130158.40-873956.3	13015862-8739562	9.015	5.7984	0.166	49.8709	8.200	7.958	7.861	-27.1	-13.0	5911	F8 V	...	EA
J131855.21-883257.6	13191646-8833012	11.205	6.5312	0.012	49.4870	9.559	8.745	8.557	-11.4	-3.9	...	...	...	SP*
J132103.23-872921.2	13212444-8729485	12.358	4.8223	0.051	52.5461	11.508	11.107	11.021	-19.9	-3.3	...	...	...	ELL*
J132322.01-881600.1	13234810-8816047	12.173	2.5109	0.284	51.5760	11.179	10.807	10.707	-7.7	-7.7	...	...	...	EB
J132809.75-875254.4	13282879-8753093	9.482	11.5647	0.023	57.7163	7.381	6.529	6.209	-8.8	-7.5	5845	M4 III	...	SP*
J134947.07-884614.3	13500355-8846131	10.022	14.3600*	0.042	52.9529	8.868	8.279	8.178	-4.3	-0.6	4257	K2 III	...	SP*
J135256.76-885416.9	13531738-8854152	12.658	0.2669	0.453	49.3671	12.047	11.575	11.493	-18.9	-25.9	...	...	...	EW
J142038.37-881430.6	14205144-8814339	12.561	0.4009	0.096	49.5236	11.915	11.621	11.585	-12.2	6.8	...	...	...	EW
J142524.87-881448.5	14253827-8814545	13.759	9.6182	0.101	51.7922	12.529	12.014	11.900	-2.0	-2.7	...	...	...	ELL*
J142848.24-883844.0	14290452-8838436	12.087	0.6462	0.651	49.8953	11.297	11.029	10.919	-24.6	2.0	6278	G0 V	...	RL
J142849.58-873755.4	14290144-8738164	13.519	0.1740	0.288	49.3466	12.640	12.268	12.143	-12.8	-14.3	...	...	...	EW*
J143139.84-881735.5	14315405-8817399	10.586	6.1315	0.012	50.4560	8.606	7.815	7.480	-4.9	-4.6	...	...	...	SP*
J145104.85-885156.0	14512053-8851540	12.340	6.2589	0.029	52.2014	11.301	10.944	10.889	-10.5	-13.4	...	...	...	ELL*
J145412.85-872039.4	14542131-8721051	9.749	...	0.652	...	7.183	6.246	5.893	-1.0	-4.0	...	...	...	IR
J152129.10-884201.5	15213927-8841598	12.980	20.7532	0.068	50.1212	11.782	11.269	11.223	3.8	5.8	...	...	...	BY*
J152502.18-882314.8	15251139-8823155	12.797	7.3767	0.055	55.8932	11.790	11.467	11.416	-13.3	-12.2	...	...	...	ELL*
J152834.73-882144.4	15284138-8821445	13.533	0.1579	0.074	49.3467	12.791	12.520	12.457	-1.5	-6.0	...	...	...	DSCT*
J153452.62-881610.5	15350038-8816128	12.116	...	0.941	...	7.688	6.503	5.668	-2.5	1.3	...	...	...	IR
J154425.02-885422.6	15443872-8854193	13.490	2.9192	0.061	51.9184	12.603	12.264	12.196	-0.1	3.2	...	...	...	GD*
J155703.16-872949.7	15570550-8730054	11.897	3.1114	0.067	51.8113	10.388	9.806	9.583	9.2	2.9	...	...	J155706.8-872949	EA
J155906.59-880038.5	15591767-8800431	14.139	6.8506	0.225	55.2989	13.230	12.835	12.752	0.6	-22.4	...	...	...	EA
J160803.46-875902.8	16075690-8759103	11.749	1.1855	0.024	50.0379	11.193	10.828	10.641	-26.0	-39.6	...	...	...	GD*
J163136.87-874001.4	16313713-8740079	12.048	10.7779	0.125	57.9673	11.163	10.780	10.642	15.2	-4.6	...	...	...	EA
J163215.16-871600.1	16321321-8716168	12.921	37.5330	0.375	56.0749	11.547	11.033	10.868	3.3	-2.8	...	...	...	DCEP*
J163700.01-884327.6	16370926-8843243	11.213	35.7535	0.070	78.4301	10.546	10.234	10.153	10.7	2.3	5618	G0 V	...	SP*
J164403.38-883823.4	16441088-8838200	10.996	18.7200*	0.018	50.5079	10.031	9.643	9.569	-66.4	-85.2	5410	K0 V	...	BY*
J170349.12-895144.9	17052321-8951438	9.658	26.6238	0.042	51.9534	7.593	6.704	6.385	2.2	-3.7	5752	M3 II	...	SP*
J171044.85-873001.7	17104277-8730093	10.549	3.2640	0.062	52.1097	9.074	8.509	8.360	1.7	-46.1	4321	K7 V	J171044.0-873015	BY*
J171319.35-874223.4	17131874-8742288	9.478	59.3650	0.138	97.9704	8.019	7.398	7.301	5.2	-21.2	4574	K2 III	...	SP*
J171340.74-882454.2	17134293-8824527	11.069	20.6600	0.063	60.2409	8.955	8.085	7.795	-7.0	1.6	...	...	...	SP*
J171536.58-890047.0	17154534-8900429	10.770	0.0226	0.006	49.3119	10.095	10.023	9.947	0.4	-23.5	7133	F02 IV	...	DSCT*
J171833.73-881247.8	17183575-8812475	13.424	42.0320	0.426	84.1776	12.047	11.450	11.308	0.3	-19.5	...	...	...	BY*

Table 1—Continued

CSTAR ID CSTAR+	2MASS ID 2MASS+	i (mag)	Period (days)	Amplitude (mag)	T_0 (2454500.0+)	J (mag)	H (mag)	K (mag)	μ_α (mas yr^{-1})	μ_δ (mas yr^{-1})	$T_{\rm eff}$ (K)	Sp.Type	*ROSAT* ID 1RXS+	Type
J173643.51-881411.8	17364589-8814105	11.286	0.0762	0.012	49.3090	10.573	10.448	10.443	0.6	-12.78	7458	F2 III	...	DSCT*
J174720.97-884612.8	17472865-8846094	11.848	0.6208	0.026	49.8218	9.992	9.386	9.072	-4.3	-26.5	...	M3.5	J174721.0-884615	BY*
J175111.31-880950.1	17511318-8809489	10.621	12.1950*	0.036	56.6081	8.357	7.515	7.153	0.2	-11.0	...	...	...	SP*
J175519.53-890743.2	17552078-8907435	14.771	0.3481	0.252	49.6733	14.079	13.819	13.658	-15.0	-2.0	...	...	...	EW*
J175900.08-880134.4	17590140-8801333	11.729	38.8530	0.087	76.6824	9.206	8.223	7.930	4.6	0.7	...	...	...	SP*
J180812.33-881806.1	18081512-8818030	10.788	2.8428	0.012	50.1137	9.910	9.579	9.544	3.8	-45.5	5749	G5 V	...	ELL*
J182144.99-893627.0	18223449-8936228	11.420	2.7821	0.024	49.9588	10.969	10.741	10.670	11.4	5.8	4192	F8 V	...	GD*
J182856.91-883236.5	18290468-8832322	13.244	0.5730	0.495	49.4171	12.312	12.315	12.147	3.8	-6.0	...	...	...	RL
J183051.60-884322.6	18305770-8843175	9.836	9.9119	0.029	53.8505	9.067	8.813	8.755	-7.6	-48.7	6033	F5	...	TR
J183527.50-883351.8	18353905-8833459	11.941	12.5012	0.020	56.4167	11.366	10.922	10.824	5.7	12.9	...	...	...	BY*
J184819.30-874319.2	18482345-8743164	11.463	0.8417	0.048	49.3579	10.651	10.483	10.415	9.5	-12.4	6212	F6 V	...	GD
J185830.92-881300.6	18583595-8812554	11.718	...	0.166	...	10.073	9.443	9.251	6.4	-22.5	...	...	...	IR*
J190015.81-884758.9	19002303-8847536	10.851	...	0.267	...	8.613	7.636	7.415	9.9	-2.9	...	...	...	IR
J190804.00-884924.1	19081282-8849184	10.047	1.6786	0.009	50.1136	9.074	8.837	8.700	-3.8	1.0	5517	G5 V	...	ELL*
J191151.31-882720.6	19115805-8827146	10.290	88.3855	0.032	69.6197	9.013	8.453	8.355	19.7	-11.9	...	...	...	SP*
J191320.83-882203.2	19132936-8821562	12.781	0.1518	0.071	49.3609	11.737	11.368	11.308	2.9	-31.1	...	...	...	DSCT
J191743.69-885117.2	19175287-8851110	11.809	0.3720	0.072	49.3506	10.769	10.395	10.279	23.5	-19.5	4808	G5 III	...	EW
J191957.22-881410.4	19201020-8814041	13.692	6.3922	0.112	55.6193	12.377	11.906	11.789	3.8	2.0	...	...	...	BY*
J192750.74-881332.7	19275809-8813263	8.613	...	0.263	...	5.144	4.016	3.674	2.0	-19.9	...	...	...	IR
J193309.49-890028.6	19332206-8900229	8.744	...	0.268	...	6.256	5.337	5.004	-6.6	-6.3	7026	M5 III	...	IR
J193320.64-884852.7	19333006-8848452	12.770	23.3421	0.060	58.8613	11.248	10.648	10.502	24.8	-60.7	...	...	...	BY*
J193823.64-885104.2	19382923-8850562	12.882	6.7525	0.356	49.4261	12.081	11.705	11.657	-102.0	74.9	...	...	...	EA
J194257.00-874701.2	19430559-8746524	14.062	0.5812	0.624	49.5479	13.070	12.847	12.722	2.8	-11.3	...	...	...	RL
J194331.61-881928.3	19434164-8819208	13.389	0.1369	0.043	49.3705	12.450	12.145	12.066	11.3	2.0	...	...	...	DSCT*
J194842.63-890720.3	19485691-8907144	10.857	4.8360	0.016	50.6935	10.198	10.089	10.036	4.8	-17.1	6789	A	...	ACV*
J195017.85-874455.3	19502673-8744506	12.814	0.4164	0.261	49.4784	12.593	12.229	12.167	11.3	-62.1	...	...	...	EW
J195302.98-892251.1	19532171-8922462	10.438	...	0.292	...	6.815	5.847	5.485	5.1	18.8	...	...	...	IR
J200208.81-880300.1	20021882-8802499	11.964	19.1496	0.157	62.6000	10.993	10.656	10.565	12.1	-13.2	3732	G8 IV	...	EA
J202830.07-874616.5	20282961-8746163	11.808	2.1926	0.320	51.3740	10.690	10.284	10.178	14.6	-18.4	4533	G5 III	...	EA
J203422.01-893408.1	20345196-8934032	12.813	2.3847	0.054	51.3896	12.042	11.857	11.805	-4.9	3.2	...	...	...	GD*
J211154.63-872452.5	21120834-8724251	9.130	0.1662	0.009	49.2969	7.712	7.172	7.014	-4.3	8.4	4361	K	...	SP*
J212325.97-891804.7	21241318-8917567	13.806	0.2336	0.138	49.3235	13.631	13.376	13.445	3.5	-17.2	...	...	...	EW*
J214700.81-873934.0	21471689-8739065	12.803	0.4580	0.630	49.5727	11.972	11.654	11.630	13.0	-24.6	...	...	...	RL
J215211.11-874450.8	21522639-8744205	10.542	10.5600	0.024	57.0527	9.770	9.472	9.350	51.1	7.4	...	G8 V	...	SP*
J220358.43-882952.0	22042836-8829345	13.571	24.1180	0.176	58.6974	12.201	11.534	11.392	0.2	1.7	...	...	...	SP*

Table 1—Continued

CSTAR ID CSTAR+	2MASS ID 2MASS+	i (mag)	Period (days)	Amplitude (mag)	T_0 (2454500.0+)	J (mag)	H (mag)	K (mag)	μ_α (mas yr^{-1})	μ_δ (mas yr^{-1})	$T_{\rm eff}$ (K)	Sp.Type	*ROSAT* ID 1RXS+	Type
J220446.20-895210.9	22051862-8952065	13.046	1.9894	0.245	49.8680	11.972	11.543	11.469	-0.1	2.1	...	...	...	EB
J221144.70-873736.8	22120189-8737041	9.559	...	0.106	...	6.930	6.088	5.717	14.5	-0.8	...	M5.3 V	...	IR
J221718.53-873221.6	22173420-8731441	10.713	...	0.222	...	9.181	8.554	8.394	12.0	-7.0	...	K3 III	...	IR
J221724.60-890149.4	22174589-8901377	9.423	...	0.134	...	6.570	5.674	5.301	10.2	-6.9	...	...	...	IR
J222319.77-885356.3	22234093-8853429	9.700	0.5217	0.011	49.7554	8.926	8.778	8.716	4.1	8.8	8200	A5	...	GD
J222801.46-883157.4	22282259-8831408	14.115	3.8174	0.131	49.4741	13.032	12.391	12.254	-12.1	-17.2	...	...	...	BY*
J223650.46-872928.7	22370727-8728498	11.608	0.8484	0.532	50.0378	10.978	10.728	10.689	15.5	-6.2	...	F5 III	...	EW
J224540.82-880525.7	22460178-8804588	13.821	7.7602	0.300	49.9507	12.811	12.463	12.411	6.9	-5.1	...	...	...	EA
J225258.24-893847.5	22531047-8938406	13.737	0.1333	0.111	49.2911	12.951	12.456	12.384	2.8	16.3	...	...	...	BY*
J230109.68-872305.8	23012368-8722200	9.488	...	0.082	...	7.395	6.481	6.209	3.3	2.8	...	M3 II	...	IR
J230127.51-892509.2	23013213-8925013	13.979	2.9277	0.104	50.7695	12.771	12.367	12.168	-3.1	0.2	...	...	...	BY*
J230301.41-893946.1	23031966-8939404	10.105	5.6812	0.007	50.1432	9.309	9.078	8.997	27.0	17.3	4750	K0	...	BY*
J230317.73-883235.2	23034004-8832137	10.261	...	0.110	...	7.864	6.945	6.606	4.4	10.1	...	...	...	IR
J231515.57-880802.8	23153607-8807338	10.734	20.6600*	0.028	63.9597	8.711	7.801	7.529	6.4	-3.6	...	...	...	SP*
J233039.10-873514.8	23303932-8735148	8.631	...	0.092	...	6.865	6.057	5.832	7.0	-0.3	...	M1 III	...	IR
J235214.93-880421.5	23523066-8803493	13.860	0.1220	0.069	49.3172	12.959	12.647	12.581	-6.8	-0.5	...	...	...	ELL*

Notes. Objects are listed in order of increasing right ascension. The column descriptions are as follows: Col. (1): CSTAR identifier of variability. Col. (2): 2MASS identifier of variability. Col. (3): Median i apparent magnitude. Col. (4): Period of variability (only for periodic variables). Improved periods are given for 7 known variables in the field - such cases are marked with asterisks. Col. (5): Amplitude of variability. Col. (6): Times of minimum brightness of periodic variability (if available). Col. (7-9): JHK near-infrared magnitudes from the 2MASS catalog. Col. (10, 11): Proper motion in right ascension and declination from the PPMXL catalog. Col. (12, 13): Effective temperature and spectral type from the VizieR database (if available). Col. (14): *ROSAT* identifier of variability. Col. (15): Type of variability: ACV, α^2 Canum Venaticorum variables; BY, BY Draconis-type variables; CEP, Cepheid variables; DCEP, δ Cephei-type variables; DSCT, δ Scuti-type variables; EA, Algol-type eclipsing binaries; EB, β Lyrae-type eclipsing binaries; EW, W Ursae Majoris-type eclipsing binaries; ELL, Rotating ellipsoidal variables; GD, γ Doradus variables; IR, Irregular variables; RL, RR Lyrae-type variables; SP, Spotted variables that are not classified into a particular class; TR, Transit-like events. Improved classifications are given for 120 known variables in the CSTAR field based on their stellar information (color, proper motion, effective temperature, luminosity class, spectral type, and X-ray activity), as well as the noteworthy features (shape, period, and amplitude) of their light curves; Such cases are marked with asterisks.

Table 2. Catalog of Newly Discovered Variables in the CSTAR Field

CSTAR ID CSTAR+	2MASS ID 2MASS+	i (mag)	Period (days)	Amplitude (mag)	T_0 (2454500.0+)	J (mag)	H (mag)	K (mag)	μ_α (mas yr^{-1})	μ_δ (mas yr^{-1})	$T_{\rm eff}$ (K)	Sp.Type	*ROSAT* ID 1RXS+	Type
J005803.18-874048.3	00582819-8739496	12.997	2.5200	0.129	52.6134	12.299	11.830	11.708	4.8	5.7	...	...	...	BY
J010723.08-873113.8	01072961-8730248	11.806	2.4340	0.043	52.5037	10.894	10.641	10.520	16.9	14.7	...	...	...	GD
J013547.71-882408.6	01361199-8823525	12.204	2.4037	0.021	50.5770	11.676	11.211	11.077	-75.4	31.3	...	...	...	BY
J014112.64-874443.9	01412495-8743549	9.863	13.2200	0.036	54.5297	7.620	6.750	6.420	3.5	6.7	...	...	...	SP
J015902.26-875744.5	01590860-8757025	10.711	8.8030	0.017	49.3791	9.538	9.095	8.962	17.9	43.5	4603	G5 III	...	ELL
J020532.02-870950.8	02053110-8708532	9.818	...	0.155	...	7.133	6.212	5.856	7.7	4.7	...	...	...	IR
J021345.72-875233.2	02135122-8751490	9.428	0.1179	0.007	49.3093	8.583	8.399	8.388	23.9	-1.7	7200	F0	...	DSCT
J022526.86-871306.8	02252557-8712132	13.306	0.4569	0.371	50.4089	12.525	12.264	12.212	2.6	-0.6	...	...	...	EW
J025231.75-872106.5	02522563-8720209	11.860	...	0.558	...	5.575	3.903	2.897	-3.6	24.9	...	...	...	IR
J030022.48-880345.0	03003494-8802599	10.123	...	0.616	...	6.841	6.033	5.620	7.6	2.7	...	M	...	IR
J031345.26-891520.2	03142715-8915069	13.036	0.3447	0.165	49.3979	12.832	12.454	12.345	18.4	-3.0	...	...	...	EW
J032945.42-881515.7	03293970-8814478	7.958	8.1700	0.012	55.4186	7.065	6.765	6.68	85.0	77.8	5707	K0/2 III	J032928.0-881420	ELL
J035740.12-872951.5	03572983-8729165	7.739	...	0.105	...	5.843	4.985	4.670	0.7	2.1	5297	M0	...	IR
J043909.99-880924.6	04390019-8809025	9.923	4.2317	0.011	51.2376	9.057	8.743	8.657	29.1	33.5	5863	G5 IV	J043928.7-880901	ELL
J045457.50-873905.0	04544817-8738470	11.115	12.7500	0.039	51.0847	10.450	10.094	9.999	-7.3	23.6	4744	K0 V	...	BY
J045747.11-870853.0	04573780-8708222	10.495	...	0.165	...	8.11	7.218	6.878	-11.3	15.4	...	...	...	IR
J051458.55-893236.7	05142450-8932238	14.412	0.3582	0.299	49.4550	14.024	13.581	13.368	6.0	15.5	...	...	...	EW
J055356.39-890038.4	05540835-8900302	9.073	...	0.064	...	7.038	6.177	5.752	-10.2	1.7	...	...	...	IR
J060135.81-880220.6	06012720-8802104	9.992	1.3658	0.009	49.9398	9.059	8.651	8.681	8.0	38.4	5649	K0	...	BY
J061755.18-873951.9	06174974-8739458	13.329	3.0230	0.190	52.3440	12.299	11.926	11.829	7.4	21.0	...	...	...	EA
J061948.66-872043.4	06194255-8720381	12.349	0.4914	0.227	49.4856	11.579	11.327	11.255	-4.1	12.1	...	...	...	EW
J063003.90-872239.0	06295719-8722303	11.915	0.3522	0.081	49.6722	11.548	11.225	11.07	-2.4	-8.3	...	...	...	GD
J064746.85-893148.6	06471157-8931358	13.463	0.1770	0.116	49.3533	13.152	12.791	12.726	3.0	-14.0	...	...	...	DSCT
J065329.31-883407.0	06532219-8834040	9.492	2.6828	0.004	51.1019	7.847	7.137	6.892	4.3	4.3	4136	K5 III	...	ELL
J065511.61-883610.7	06550550-8836088	12.572	27.3200	0.067	55.4381	11.616	11.291	11.217	13.5	28.4	...	...	...	SP
J070159.93-871103.2	07020167-8711076	12.192	...	0.317	...	9.355	8.352	8.005	10.0	9.7	...	...	...	IR
J072339.73-885107.3	07233485-8851068	8.862	1.6155	0.013	49.8242	8.485	8.480	8.453	-18.4	22.1	9103	B9 V	...	ACV
J073405.24-874035.4	07341910-8740553	13.199	0.3311	0.168	49.5406	12.991	12.706	12.686	4.9	0.2	...	...	...	EW
J074725.01-882946.0	07473154-8829582	13.941	0.1532	0.205	49.4236	13.851	13.323	13.196	-8.8	4.4	...	...	...	BY
J075334.71-872702.5	07533989-8727214	7.872	...	0.368	...	4.606	3.473	3.108	9.4	-9.2	9396	M7 III	...	IR
J085236.32-873540.6	08524613-8736008	10.713	7.6100	0.024	51.4599	9.896	9.610	9.521	-26.0	19.6	5945	F8 V	...	ELL
J091511.48-871355.8	09152603-8714302	10.349	...	0.161	...	7.408	6.437	5.969	-2.0	-2.4	...	...	...	IR
J092000.67-871417.4	09202970-8714488	11.750	1.3760	0.051	50.5983	10.798	10.224	10.099	-2.06	5.9	...	...	...	SP
J093325.93-865454.6	09334218-8655344	12.633	4.4255	0.473	52.2783	11.458	11.096	11.008	-1.8	11.4	...	...	...	EA
J093357.77-870002.0	09341289-8700397	11.136	0.7137	0.122	49.6051	9.952	9.409	9.322	3.1	29.5	4662	K0 IV	J093359.9-870018	BY

Table 2—Continued

CSTAR ID CSTAR+	2MASS ID 2MASS+	i (mag)	Period (days)	Amplitude (mag)	T_0 (2454500.0+)	J (mag)	H (mag)	K (mag)	μ_α (mas yr^{-1})	μ_δ (mas yr^{-1})	$T_{\rm eff}$ (K)	Sp.Type	*ROSAT* ID 1RXS+	Type
J094416.17-871300.8	09443076-8713347	7.250	...	0.127	...	4.599	3.49	3.136	11.6	4.2	7243	M6 III	...	IR
J094958.41-872443.9	09501698-8725167	8.569	...	0.088	...	6.338	5.449	5.147	-1.6	5.8	6325	M5 III	...	IR
J095005.83-882010.1	09502433-8820201	12.175	27.0200	0.089	55.7759	10.571	9.813	9.639	-7.6	13.6	...	...	...	SP
J095045.98-874516.9	09510307-8745382	9.697	24.6300	0.032	62.9607	8.051	7.311	7.087	-14.9	9.1	3385	K5 III	...	SP
J100225.51-880053.9	10025017-8801166	14.210	0.1588	0.238	50.3830	14.040	13.636	13.581	-5.2	32.7	...	...	J100421.7-880147	BY
J110754.27-870108.3	11081616-8701540	12.173	0.5116	0.325	49.7146	10.935	10.505	10.355	-14.8	21.6	...	...	...	EW
J111323.25-872425.7	11133274-8724345	13.274	0.3315	0.537	49.4655	12.39	12.086	12.018	-7.5	-.5	...	...	...	SP
J112013.47-870327.3	11203606-8704105	8.362	...	0.323	...	4.968	4.132	3.640	-8.7	-4.7	...	...	...	IR
J113905.26-870840.1	11392518-8709264	10.875	...	0.952	...	7.825	7.071	6.555	0.9	1.7	...	M	...	IR
J120806.96-871541.8	12083046-8716180	11.719	1.9511	0.046	51.2041	10.94	10.719	10.639	-5.0	-4.0	3339	G5 V	...	ELL
J122723.61-871548.9	12274655-8716251	11.508	18.7900	0.141	66.0030	8.579	7.671	7.315	-11.3	3.5	...	...	...	SP
J125329.92-872651.4	12535229-8727208	7.636	...	0.191	...	5.516	4.296	3.948	1.9	10.5	9360	M5 III	...	IR
J133401.71-873625.0	13342028-8736468	10.545	0.1357	0.006	49.3542	9.729	9.544	9.466	-10.0	-9.4	6255	F6 V	...	DSCT
J140133.20-880215.7	14015518-8802247	10.931	5.4626	0.012	51.9950	10.217	9.87	9.779	-20.6	-8.6	4332	G8 IV	...	BY
J141946.97-885649.1	14201255-8856440	12.956	0.7206	0.036	49.8531	12.417	12.122	12.04	14.8	10.4	...	...	...	GD
J143433.97-894619.0	14353106-8946181	6.306	2.0166	0.127	49.3314	2.645	1.797	1.485	-8.5	-8.5	3530	M3 III	...	EA
J144250.43-873519.4	14430782-8735405	10.638	22.1200	0.085	59.5769	8.575	7.685	7.301	-6.6	-14.2	5951	F5 V	...	CEP
J145034.77-881937.2	14504684-8819403	8.518	4.2922	0.007	52.6390	6.832	6.053	5.821	-20.6	-6.9	4504	K2	...	ELL
J145941.12-882233.7	14595189-8822358	8.084	3.0470	0.011	52.2466	6.701	6.179	5.959	12.9	-18.4	4420	K2 III	...	EA
J150525.99-873549.4	15053474-8736055	12.319	3.7260	0.101	52.5513	11.487	11.192	11.15	-10.3	-13.8	3808	G2 V	...	EA
J160642.76-870827.2	16064306-8708500	12.178	3.5349	0.128	52.2063	10.734	10.153	10.006	-9.3	-51.2	...	...	...	BY
J161552.75-873042.5	16154620-8729326	12.768	0.5585	0.638	49.3117	10.672	10.077	9.996	-5.2	-8.6	...	...	...	RL
J165107.45-870755.4	16510558-8708124	6.959	...	0.196	...	4.967	3.781	3.55	-2.2	-4.0	3442	M3	...	IR
J170228.67-870260.0	17022757-8703176	9.930	...	0.199	...	8.081	7.211	7.018	-10.1	-2.6	4589	M3 III	...	IR
J171307.62-875127.5	17130808-8751309	8.113	8.3451	0.010	55.3413	6.402	5.638	5.377	8.1	-25.5	4420	K2	...	ELL
J172404.77-884916.9	17241282-8849115	12.478	0.1889	0.034	49.3761	11.801	11.531	11.533	4.3	-0.2	...	...	...	DSCT
J181721.88-870557.6	18171493-8705366	10.807	0.3528	0.125	49.6542	10.356	9.932	9.833	-61.1	-120.4	5369	K0 V	...	EW
J182043.98-872903.6	18204533-8729061	8.520	...	0.102	...	6.462	5.570	5.287	5.7	-9.5	6014	M4 III	...	IR
J182306.70-872026.5	18230769-8720275	13.669	0.1470	0.113	49.4136	12.925	12.817	12.726	-1.2	-16.3	...	...	...	DSCT
J200606.27-871334.8	20061908-8713331	13.685	0.4232	0.293	50.2762	13.366	13.140	13.093	-0.5	-14.9	...	...	...	EW
J202630.55-881144.0	20264378-8811323	11.886	2.1617	0.016	51.1285	11.129	10.960	10.937	8.6	-8.8	3635	F8 V	...	GD
J202830.67-874328.0	20283749-8743056	13.470	0.5235	0.288	49.4847	13.253	13.07	13.083	2.6	-19.4	...	...	...	RL
J203353.38-871607.0	20340201-8715499	13.147	2.0310	0.320	49.2911	12.937	12.715	12.683	5.5	-12.2	...	...	...	DCEP
J203718.65-880651.6	20373265-8806383	8.920	0.1546	0.003	49.3173	8.267	8.166	8.088	3.9	-3.5	7419	A1 V	...	DSCT
J204420.50-871354.9	20443167-8713334	10.048	...	0.237	...	7.798	6.823	6.506	10.1	3.0	...	...	...	IR

Table 2—Continued

CSTAR ID CSTAR+	2MASS ID 2MASS+	i (mag)	Period (days)	Amplitude (mag)	T_0 (2454500.0+)	J (mag)	H (mag)	K (mag)	μ_α (mas yr^{-1})	μ_δ (mas yr^{-1})	$T_{\rm eff}$ (K)	Sp.Type	*ROSAT* ID 1RXS+	Type
J205355.20-890353.3	20541080-8903450	10.027	1.8570	0.018	51.0645	8.798	8.318	8.178	41.4	-31.1	4388	K2 III	...	EA
J210708.00-892015.3	21063078-8920084	12.045	24.5100	0.062	53.9480	11.014	10.201	10.003	7.9	2.9	...	...	...	SP
J212908.01-872941.9	21292608-8729118	13.458	1.9240	0.331	50.3511	12.836	12.312	12.265	17.2	-24.5	...	...	...	BY
J223815.10-871009.5	22383291-8710260	11.685	0.1615	0.280	49.4776	9.708	9.435	9.380	-24.1	-11.6	...	F8 V	...	DSCT
J224453.92-870528.8	22450750-8704303	12.323	...	0.240	...	10.479	9.744	9.493	3.9	0.7	...	...	...	IR
J224645.19-881953.5	22470496-8819300	8.502	6.1315	0.010	51.1612	7.704	7.559	7.459	74.1	-34.2	6440	F5 V	J224723.5-881931	ELL
J230048.11-870410.9	23010623-8703109	10.247	...	0.505	...	6.864	6.024	5.574	0.8	-.6.6	3611	M	...	IR
J230224.56-872612.7	23025750-8725269	10.907	...	0.127	...	9.607	8.800	8.596	-3.7	-4.2	...	...	...	IR
J231844.03-870314.0	23191054-8702139	8.238	...	0.283	...	5.216	4.369	4.039	8.4	-2.2	...	M6 III	...	IR
J233018.21-873602.6	23303932-8735148	8.572	...	0.104	...	6.865	6.057	5.832	7.0	-0.3	...	M1 III	...	IR
J233305.33-881550.2	23332481-8815220	10.318	1.9385	0.006	50.9775	8.603	7.846	7.607	12.1	-2.3	...	K5 III	...	ELL
J234721.33-875625.3	23474168-8755475	12.790	0.1138	0.025	49.4081	11.657	11.217	11.158	-9.4	-6.4	...	...	...	BY
J235709.09-882520.4	23572768-8824543	12.370	3.0980	0.065	50.8865	11.488	11.213	11.101	7.4	-6.9	...	...	...	TR

Notes. Objects are listed in order of increasing right ascension. The column descriptions are as follows: Col. (1): CSTAR identifier of variability. Col. (2): 2MASS identifier of variability. Col. (3): Median i apparent magnitude. Col. (4): Period of variability (only for periodic variables). Col. (5): Amplitude of variability. Col. (6): Times of minimum brightness of periodic variability (if available). Col. (7-9): JHK near-infrared magnitudes from the 2MASS catalog. Col. (10, 11): Proper motion in right ascension and declination from the PPMXL catalog. Col. (12, 13): Effective temperature and spectral type from the VizieR database (if available). Col. (14): *ROSAT* identifier of variability. Col. (15): Type of variability: ACV, α^2 Canum Venaticorum variables; BY, BY Draconis-type variables; CEP, Cepheid variables; DCEP, δ Cephei-type variables; DSCT, δ Scuti-type variables; EA, Algol-type eclipsing binaries; EW, W Ursae Majoris-type eclipsing binaries; ELL, Rotating ellipsoidal variables; GD, γ Doradus variables; IR, Irregular variables; RL, RR Lyrae-type variables; SP, Spotted variables that are not classified into a particular class; TR, Transit-like events.

Table 3. Missed Variables during Our Variability Search

CSTAR ID CSTAR+	2MASS ID 2MASS+	i (mag)	Period (days)	Δi_{90} (mag)	T_0 (2454500.0+)	J (mag)	H (mag)	K (mag)	μ_α (mas yr^{-1})	μ_δ (mas yr^{-1})	$T_{\rm eff}$ (K)	Sp.Type	*ROSAT* ID 1RXS+	Type
J004526.78-882521.3	00452677-8825210	11.57	34.5266	...	...	10.454	10.058	9.970	21.5	0.1	...	...	...	U
J005607.00-884217.9*	00560824-8842175	11.36	7.9944	0.04	...	10.278	9.773	9.672	21.7	4.4	...	...	...	MP
J010804.79-874759.1	01080487-8747588	13.87	15.8462	...	...	12.432	11.929	11.727	8.6	7.2	...	...	...	U
J021102.80-892250.3	02110223-8922496	10.27	6.6230	0.03	...	8.441	7.644	7.380	9.1	31.1	...	...	...	MP
J025225.60-872021.5	02522563-8720209	13.66	...	1.03	...	5.575	3.903	2.897	-3.6	24.9	...	...	...	IR
J030117.31-892430.2	03011730-8924295	12.38	5.7673	0.05	785.6845	11.321	10.930	10.842	16.4	30.6	...	...	...	TR
J031122.58-891513.6	03112278-8915130	14.08	0.1723	...	55.6132	12.832	12.454	12.345	18.4	-3.0	...	...	...	EC
J034410.88-885209.5	03441024-8852092	11.19	21.4962	0.03	...	9.515	8.677	8.477	7.4	3.2	...	...	...	MP
J051549.62-881751.5	05155008-8817516	10.21	11.4628	0.04	...	8.452	7.617	7.389	2.4	13.7	4750	M1 III	...	MP
J053059.30-883004.7	05305863-8830041	13.52	9.6756	...	...	12.462	12.085	11.982	19.9	11.3	...	...	...	U
J055034.20-890646.2*	05503182-8906455	12.94	0.7989	0.08	785.3570	12.167	12.03	11.983	-0.1	6.0	...	...	...	U
J055530.36-875706.8*	05552966-8757064	14.02	0.7141	...	...	12.499	11.943	11.863	0.4	16.2	...	...	...	U
J062315.53-883335.4	06231441-8833351	12.68	34.7336	...	...	11.589	11.123	11.034	-0.4	-6.9	...	...	...	U
J071442.32-872225.0	07144230-8722249	11.37	...	0.07	...	10.338	9.966	9.916	-15.8	34.4	4188	K0 V		IR
J082118.73-885548.2*	08211421-8855476	13.40	9.9751	...	...	12.476	11.997	11.910	-36.6	21.0	...	...	...	U
J085151.07-891521.3	08514807-8915212	12.27	3.4818	0.05	785.5641	11.236	10.921	10.859	-9.1	0.6	...	...	...	U
J100432.92-871344.7	10043290-8713446	10.97	19.0817	0.08	...	9.038	8.138	7.861	1.2	7.3	...	...	...	MP
J105011.96-885954.1	10500911-8859540	11.78	5.7456	0.05	787.1325	9.68	9.05	8.838	-52.0	38.2	...	M3.5	...	U
J114432.67-872735.9	11443220-8727360	10.89	31.4480	0.12	...	9.023	8.095	7.859	-2.5	-3.5	...	...	...	MP
J120934.38-882959.0	12093288-8829594	11.49	17.2566	0.05	...	9.717	8.83	8.59	-12.8	-6.1	...	...	...	MP
J123049.10-890245.7	12304948-8902458	11.94	25.1254	0.03	787.7145	11.355	11.3	11.264	-23.3	-16.0	8174	A7 V	...	U
J124214.25-885905.0	12421269-8859054	12.55	13.1234	...	...	10.729	9.928	9.720	-7.0	0.5	...	...	...	DSCT
J130129.04-891347.0	13012600-8913474	13.21	6.4227	0.11	787.0902	11.738	11.143	10.986	-46.7	-18.8	...	...	...	U
J150955.59-872501.9	15095571-8725017	9.09	...	0.08	...	8.226	7.933	7.940	-37.0	-86.3	6870	F2 IV/V	...	IR
J154444.17-874635.4	15444418-8746354	8.35	...	0.09	...	7.204	6.743	6.654	-48.9	-29.8	5770	G6 V	...	IR
J172325.05-885337.3	17232555-8853378	9.99	34.4791	0.07	...	7.576	6.694	6.370	-0.9	-1.6	...	...	...	MP
J172537.17-884950.3	17253724-8849507	13.83	0.1890	0.35	785.3176	12.876	12.602	12.546	-9.0	-10.2	...	...	...	DSCT
J190233.97-873530.2	19023397-8735303	8.86	...	0.07	...	7.367	6.648	6.514	0.6	-21.9	4750	K0	...	IR
J205731.47-890350.3	20573329-8903503	12.36	1.8576	0.33	786.0597	11.236	10.955	10.929	17.4	-16.3	...	...	...	ED
J211945.21-882817.7	21194610-8828175	13.39	43.6389	0.16	...	12.054	11.563	11.447	13.19	-25.55	...	...	...	MP
J231645.97-875416.6	23164652-8754161	11.95	8.7540	0.07	...	10.883	10.322	10.202	29.6	-8.2	...	...	...	MP
J233511.99-892751.8	23351496-8927514	14.78	0.4658	1.23	785.3995	13.375	13.057	13.047	-3.5	-7.2	...	...	...	RL
J235727.17-882454.5	23572768-8824543	12.44	6.1985	0.06	788.5551	11.488	11.213	11.101	7.4	-6.9	...	...	...	ED

Notes. Objects are listed in order of increasing right ascension. The column descriptions are as follows: Col. (1): CSTAR identifier of variability, stars marked with asterisks may suffer from 1-d aliases and thus their variability is not confirmed in this study . Col. (2): 2MASS identifier of variability. Col. (3): Median i apparent magnitude. Col. (4): Period of variability (only for periodic variables). Col. (5): 1.64 standard deviation (90% confidence interval) of the light curve. Col. (6): Times of minimum brightness of periodic variability (if available). Col. (7-9): JHK near-infrared magnitudes from the 2MASS catalog. Col. (10, 11): Proper motion in right ascension and declination from the PPMXL catalog. Col. (12, 13): Effective temperature and spectral type from the VizieR database (if available). Col. (14): *ROSAT* identifier of variability. Col. (15): Type of variability: DSCT, δ Scuti-type variables; EC, Contact eclipsing binaries; ED, Detached eclipsing binaries; IR, Irregular variables; MP, Multi-periodic variables; RL, RR Lyrae-type variables; TR, Transit-like events; U, Unclassified variables.

Table 4. Distribution of Variables in the CSTAR Field by Type.

Type	Recovered Variables	Newly Discovered Variables	Total Variables
ACV	2	1	3
BY	35	11	44
CEP	1	1	2
DCEP	2	1	3
DSCT	10	7	17
EA	21	6	27
EB	3	0	3
EW	20	8	28
ELL	13	10	23
GD	12	4	16
IR	30	23	53
RL	6	2	8
SP	34	8	42
TR	2	1	3
Total	191	83	274

Notes. The first column is an alphabetical type of variability: ACV, α^2 Canum Venaticorum variables; BY, BY Draconis-type variables; CEP, Cepheid variables; DCEP, δ Cephei-type variables; DSCT, δ Scuti-type variables; EA, Algol-type eclipsing binaries; EB, β Lyrae-type eclipsing binaries; EW, W Ursae Majoris-type eclipsing binaries; ELL, Rotating ellipsoidal variables; GD, γ Doradus variables; IR, Irregular variables; RL, RR Lyrae-type variables; SP, Spotted variables that are not classified into a particular class; TR, Transit-like events.